OXYGEN FUGACITY ACROSS TECTONIC SETTINGS

Elizabeth Cottrell[1,1], Suzanne Birner[2,2], Maryjo Brounce[3,3], Fred Davis[4,4], Laura Waters[5,5], and Katherine Kelley[6,6]

[1]National Museum of Natural History, Smithsonian Institution
[2]Berea College
[3]University of California Riverside
[4]University of Minnesota Duluth
[5]New Mexico Institute of Mining and Technology
[6]University of Rhode Island, Graduate School of Oceanography

November 30, 2022

Abstract

Experiment and observation have established the centrality of oxygen fugacity (fO2) to determining the course of igneous differentiation, and so the development and application of oxybarometers have proliferated for more than half a century. The compositions of mineral, melt, and vapor phases determine the fO2 that rocks record, and the activity models that underpin calculation of fO2 from phase compositions have evolved with time. Likewise, analytical method development has made new sample categories available to oxybarometric interrogation. Here we compile published analytical data from lithologies that constrain fO2 (n=860 volcanic rocks - lavas and tephras and n=326 mantle lithologies- the majority peridotites) from ridges, back-arc basins, forearcs, arcs, and plumes. Because calculated fO2 varies with choice of activity model, we re-calculate fO2 for each dataset from compositional data, applying the same set of activity models and methodologies for each data type. Additionally, we compile trace element concentrations (e.g. vanadium) which serve as an additional fO2-proxy. The compiled data show that, on average, volcanic rocks and mantle rocks from the same tectonic setting yield similar fO2s, but mantle lithologies span a much larger range in fO2 than volcanics. Multiple Fe-based oxybarometric methods and vanadium partitioning vary with statistical significance as a function of tectonic setting, with fO2 ridges < back arcs < arcs. Plume lithologies are more nuanced to interpret, but indicate fO2s ? ridges. We discuss the processes that may shift fO2 after melts and mantle lithologies physically separate from one another. We show that the effects of crystal fractionation and degassing on the fO2 of volcanics are smaller than the differences in fO2 between tectonic settings and that effects of subsolidus metamorphism on the fO2 values recorded by mantle lithologies remain poorly understood. Finally, we lay out challenges and opportunities for future inquiry.

3

Oxygen Fugacity Across Tectonic Settings

Elizabeth Cottrell[1], Suzanne K. Birner[2], Maryjo Brounce[3], Fred A. Davis[4], Laura E. Waters[5], and Katherine A. Kelley[6]

ABSTRACT

Experiment and observation have established the centrality of oxygen fugacity (fO_2) to determining the course of igneous differentiation, and so the development and application of oxybarometers have proliferated for more than half a century. The compositions of mineral, melt, and vapor phases determine the fO_2 that rocks record, and the activity models that underpin calculation of fO_2 from phase compositions have evolved over time. Likewise, analytical method development has made new sample categories available to oxybarometric interrogation. Here we compile published analytical data from lithologies that constrain fO_2 (n=860 volcanic rocks – lavas and tephras – and n=326 mantle lithologies – the majority peridotites) from ridges, back-arc basins, forearcs, arcs, and plumes. Because calculated fO_2 varies with choice of activity model, we recalculate fO_2 for each dataset from compositional data, applying the same set of activity models and methodologies for each data type. Additionally, we compile trace element concentrations (e.g., vanadium) which serve as an additional fO_2-proxy. The compiled data show that, on average, volcanic rocks and mantle rocks from the same tectonic setting yield similar fO_2s, but mantle lithologies span a much larger range in fO_2 than volcanics. Multiple Fe-based oxybarometric methods and vanadium partitioning vary with statistical significance as a function of tectonic setting, with fO_2 ridges < back arcs < arcs. Plume lithologies are more nuanced to interpret, but indicate fO_2s ≥ ridges. We discuss the processes that may shift fO_2 after melts and mantle lithologies physically separate from one another. We show that the effects of crystal fractionation and degassing on the fO_2 of volcanics are smaller than the differences in fO_2 between tectonic settings and that effects of subsolidus metamorphism on the fO_2 values recorded by mantle lithologies remain poorly understood. Finally, we lay out challenges and opportunities for future inquiry.

[1]*Department of Mineral Sciences, National Museum of Natural History, Smithsonian Institution, Washington, DC, USA*

[2]*Division of Natural Sciences, Nursing, and Mathematics, Berea College, Berea, KY, USA*

[3]*Department of Earth and Planetary Sciences, University of California Riverside, Riverside, CA, USA*

[4]*Department of Earth and Environmental Sciences, University of Minnesota Duluth, Duluth, MN, USA*

[5]*Department of Earth and Environmental Science, New Mexico Institute of Mining and Technology, Socorro, NM, USA*

[6]*Graduate School of Oceanography, University of Rhode Island, Narragansett, RI, USA*

3.1. INTRODUCTION

The role that oxygen fugacity (fO_2) plays in producing the unique topography of Earth's surface, defined by high-standing continents and low-lying ocean basins, was recognized in the 1950s, when workers such as Kennedy (1955), Eugster (1957,1959), and Osborn (1959) established the link between fO_2 and the course of igneous differentiation. Crystallization under high fO_2 leads to the calc-alkaline magmatic series common on the continents, while crystallization under low fO_2 results in the tholeiitic magma series common in ocean basins. In order to

Magma Redox Geochemistry, Geophysical Monograph 266, First Edition.
Edited by Roberto Moretti and Daniel R. Neuville.

DOI: 10.1002/9781119473206.ch3

connect these laboratory-based insights to natural rocks, petrologists began to develop proxies for fO_2, and to apply them in earnest. Through seminal contributions such as Eugster (1959), Haggerty (1976), Christie et al. (1986), Carmichael (1991), Wood et al. (1990), Frost and Lindsley (1992), Ballhaus (1993), Canil (1997), and innumerable others, petrologists began to quantify and map the link between tectonic environment and oxygen fugacity.

3.1.1. Theoretical Background

Oxygen fugacity, or fO_2, describes the potential for an element to occur in an oxidized or reduced state – that is, with a higher or lower charge. If oxygen were an ideal gas, its chemical potential (μ) would simply be related to its partial pressure (P) via

$$\mu_{O_2} = \mu^{\circ}_{O_2} + RTln\frac{P}{P_0} \tag{3.1}$$

Where $\mu^{\circ}_{O_2}$ is the standard state chemical potential of O_2, R is the gas constant, T is the temperature in Kelvin, and P_0 is the standard state pressure of pure O_2. Because no gas, and certainly no rock, behaves as an ideal gas, we substitute fugacity (f) for partial pressure, which corrects pressure for non-ideality, much as chemical activity corrects concentration for non-ideality. The chemical potential of oxygen is then

$$\mu_{O_2} = \mu^{\circ}_{O_2} + RTln\frac{f_{O_2}}{f^{\circ}_{O_2}} = \mu^{\circ}_{O_2} + RTlnf_{O_2} \tag{3.2}$$

when $f^{\circ}_{O_2} = 1$ (the fugacity of pure O_2 at 1 bar and T of interest). In this way, we can relate the free energy of any equilibria of pure phases involving O_2 to oxygen fugacity via the change in Gibbs free energy ($\Delta G^{\circ}_{reaction}$)

$$\Delta G^{\circ}_{reaction} = -RTlnK_{eq} \tag{3.3}$$

where K_{eq} is the equilibrium constant. When P and T are specified, such equilibria of pure phases fix the activity of O_2, or "buffer" the fO_2.

3.1.2. Fe-Based Oxybarometry

Equilibria involving iron are useful because iron is the most abundant multivalent element in the solid Earth and is present in the common rock-forming minerals. For example, the oxygen fugacity of the equilibrium reaction of the pure phases fayalite goes to ferrosilite plus magnetite:

$$\underset{(fayalite)}{6Fe_2SiO_4} + \underset{(oxygen)}{O_2} \leftrightarrow \underset{(\text{ferrosilite})}{3Fe_2Si_2O_6} + \underset{(magnetite)}{2Fe_3O_4} \tag{3.4}$$

can be calculated from the free energy change of the reaction using Equation 3.3. The equilibrium constant can be written:

$$K_{eq} = \frac{\left(a^{opx}_{Fe_2Si_2O_6}\right)^3\left(a^{spl}_{Fe_3O_4}\right)^2}{\left(a^{olv}_{Fe_2SiO_4}\right)^6 f_{O_2}} \tag{3.5}$$

where $a^{mineral}_{component}$ represents the activity of the end-member component (e.g., ferrosilite) within the mineral phase (e.g., orthopyroxene). In the case of pure phases, the activity is equal to unity, and so the following relationship holds true:

$$logK_{eq} = -logf_{O_2} = \left(\frac{6\Delta G^{\circ}_{Fe_2SiO_4} - 2\Delta G^{\circ}_{Fe_3O_4} - 3\Delta G^{\circ}_{Fe_2Si_2O_6}}{ln(10)RT}\right) \tag{3.6}$$

In experimental systems, oxygen fugacity can be imposed by an invariant buffer reaction involving pure phases (activities equal to unity, for example nickel [Ni] and nickel oxide [NiO]). In natural systems, oxygen fugacity is determined by equilibria involving multi-component silicate minerals, melts, and gases; mineral phases are rarely found as pure end-member compositions. This requires us to relate mineral compositions to component activities. Accurate activity-composition models are therefore important when comparing the fO_2 recorded by a single equilibrium reaction across a wide range of compositions, and even more so when comparing the fO_2 recorded by different fO_2 equilibria – when the accuracy, and not just the precision, of each equilibrium reaction is paramount. We relate the measured compositions of natural phases to the activities of end-member components (e.g., the activity of pure magnetite in spinel, $a^{spinel}_{Fe_3O_4}$) via equations like

$$-logf_{O_2} = \left(\frac{\Delta G^{\circ}_{reaction(P,T)}}{ln(10)\,RT}\right) - 2loga^{spinel}_{Fe_3O_4} - 3loga^{opx}_{Fe_2Si_2O_6} + 6loga^{olivine}_{Fe_2SiO_4} \tag{3.7}$$

Equation 3.7 describes the spinel oxybarometer (Ballhaus et al., 1991; O'Neill & Wall, 1987; Wood & Virgo, 1989) and its form prompts a review of several important points.

Any calculation of fO_2 assumes that all phases that fix the activity of oxygen are present and in equilibrium. For example, fO_2 is not constrained by the spinel oxybarometer if orthopyroxene is absent from the assemblage (unless the activity of silica can be constrained by some other means). Likewise, the composition of magnetite records fO_2 only in the presence of ilmenite (Buddington & Lindsley, 1964). We can also see from the above equations that the activity of oxygen will rise with temperature such that it is convenient

to refer to a reference buffer. In this contribution we reference the quartz-fayalite-magnetite (QFM) buffer (Frost, 1991) because its pressure-dependence parallels adiabatic melt ascent (Kress and Carmichael, 1991), facilitating comparison of magmas equilibrated at different pressures and temperatures.

It also follows from the thermodynamic treatment above that the bulk rock ratio of ferric to total iron ($Fe^{3+}/\Sigma Fe = Fe^{3+}/[Fe^{3+} + Fe^{2+}]$) in crystalline rocks cannot be equated to oxygen fugacity, because the former varies with mineral mode (extensive property) whereas the latter varies with component activity (intensive property). In melts (and glasses), steric effects are greatly reduced, such that melt (glass) $Fe^{3+}/\Sigma Fe$ ratios can be related to fO_2; however, this does not mean that the $Fe^{3+}/\Sigma Fe$ ratios of melts vary systematically with fO_2 independent of composition. With melts too, $Fe^{3+}/\Sigma Fe$ ratios must be related to fO_2 after considering composition because oxide components in the melt can stabilize or destabilize Fe^{3+} relative to Fe^{2+} at given fO_2 (e.g., Borisov et al., 2018; Kress & Carmichael, 1991; O'Neill et al., 2018).

Based on iron's role in both setting and monitoring fO_2 (Frost, 1991; D. J. Frost & McCammon, 2008), prior Fe-based compilations of fO_2 as a function of tectonic setting have relied on either spinel oxybarometry (e.g., Ballhaus, 1993; Wood et al., 1990), magnetite-ilmenite equilibria (e.g., Frost & Lindsley, 1992), or bulk rock and/or sediment $Fe^{3+}/\Sigma Fe$ ratios (e.g., Carmichael, 1991; Lecuyer & Ricard, 1999). In this chapter, we do not compile fO_2 calculated for bulk "glass" $Fe^{3+}/\Sigma Fe$ ratios because in most cases the metadata provided in publications are absent or insufficient to ensure that the samples have not suffered post-eruptive oxidation or are free of phenocrysts, both of which have been shown to compromise the fidelity of fO_2 proxies (Bezos & Humler, 2005; Brounce et al., 2017; Cottrell & Kelley, 2011; Grocke et al., 2016; Stolper & Bucholz, 2019; Bezos et al., 2021). Further, while very convenient for generating large datasets and informing box models (e.g., Brounce et al., 2019; Canil & Fellows, 2017; Evans, this volume; Evans & Tomkins, 2011; Evans et al., 2012; Lecuyer & Ricard, 1999; Stolper & Bucholz, 2019), applications of bulk "glass" or whole rock $Fe^{3+}/\Sigma Fe$ ratios are limited because the $Fe^{3+}/\Sigma Fe$ ratios of crystalline rocks and mixtures (like cumulates and sediments) cannot be directly equated to fO_2 – as detailed above.

3.1.3. Trace-Element Oxybarometry

In addition to iron, the periodic table offers us a wealth of elements that undergo valence state changes in response to changes in fO_2. The theory that underpins trace element oxybarometry is that fO_2-driven valence state changes will result in changes to mineral-melt partition coefficients. Thus, the concentration of a multivalent trace element in melt should reflect the residual mineralogy, the melt composition, and the pressure, temperature, and oxygen fugacity of the system during melting. In this way, the power of redox-sensitive minor and trace element partitioning can be harnessed to monitor the fO_2 of geologically relevant lithologies, and can offer advantages over Fe. Trace element concentrations offer advantages because they are (i) relatively straightforward to measure and (ii) should be less susceptible than formal valence state to modification after the melt separates from the residue. A wide range of redox-sensitive elements (e.g., Ti, V, Cr, Ce, Eu, U, Mo, W, Re) are discussed separately by Mallmann et al. (2021) within this volume, and we refer the interested reader to that chapter. Several trace elements, however, have been employed to infer the fO_2 of basalt source rocks (the mantle) as a function of tectonic setting (e.g., Bali et al., 2012; Bucholz & Kelemen, 2019; Canil, 1997; Laubier et al., 2014; Lee et al., 2005; Lee et al., 2010; Lee et al., 2012; Mallmann & O'Neill, 2009; Mallmann & O'Neill, 2013; Shervais, 1982). A review of all of these studies and proxies is beyond the scope of this chapter; however, we will discuss vanadium (V) – the most widely applied of these proxies. Vanadium valence can be V^{2+}, V^{3+}, V^{4+}, or V^{5+} in geologically relevant systems. The incompatibility of V^{3+} in mantle minerals is similar to many other trivalent elements, such as the rare earth elements, Sc, Y, and Ga, while V^{4+} and V^{5+} are more highly incompatible. Therefore, with all other parameters equal, melting peridotite at higher fO_2 should result in systematically higher melt V concentrations relative to other trivalent trace elements (Canil, 1997; Lee et al., 2003, 2005).

3.1.4. Other Oxybarometers

We emphasize that there are many additional, and very valuable, proxies for fO_2 that are not yet widely applied to volcanics from arc, ocean island, and mid-ocean ridge settings, but may be in the future, such as stable isotope proxies (Dauphas et al., 2009; Nebel et al., 2015; Williams et al., 2005). Similarly, microprobe peak energies (e.g., Carroll & Rutherford, 1988) and S X-ray Absorption Near Edge Structure spectra (e.g., Fleet et al., 2005) can determine sulfur oxidation state, but analyses from both techniques can be compromised by beam damage during analysis (e.g., Klimm et al., 2012; Rowe et al., 2007; Wilke et al., 2008), leaving only a handful of vetted analyses. For these, we point the interested reader to other chapters in this volume that describe some of these approaches in detail.

3.2. SAMPLE SELECTION, METHODOLOGY, AND DESIGN OF THIS STUDY

We can envision many valid approaches for compiling fO_2 determinations from the literature. In this contribution, we focus on the oxybarometric approach and apply oxybarometers that have all been cross-calibrated at 1 atmosphere under controlled atmosphere conditions at known fO_2. We compile published compositions from Earth's ridges, back arcs, forearcs, arcs, and plumes and recalculate the fO_2 values recorded by these volcanics (lavas and tephras) and mantle lithologies (mostly peridotites). We have opted to include samples wherein the original publications provide sufficient information to recalculate fO_2 (e.g., microprobe analyses) such that we may apply a single set of activity models and methodologies to all of the compositional data collected in disparate studies. This is essential, because the fO_2 calculated from a given composition may vary by up to a log unit depending on the activity model employed (e.g., Birner et al., 2017; Herd, 2008; Wood, 1990). Further, many publications do not report the formulation of the reference buffer (for example, QFM from O'Neill [1987] vs Frost [1991] vs Myers & Eugster [1983]), such that reported fO_2s may not be comparable.

We describe our methods, including chosen activity models, in detail in our methods appendix. In brief, we include widely applied oxybarometric techniques that have documented intra-technique consistency, and which require minimal metadata: magnetite-ilmenite pairs, spinel-oxybarometry, and glass spectroscopy. For example, Davis and Cottrell (2018) show that both the spinel oxybarometric method of Wood and Virgo (1989) and the Fe^{3+}/Fe^{2+} activity model of Kress and Carmichael (1991) return the experimentally imposed fO_2 of gas-mixing experiments containing spinel, olivine, and orthopyroxene in basaltic andesite liquid. Likewise, $Fe^{3+}/\Sigma Fe$ ratios of glasses converted to fO_2 via the Kress and Carmichael (1991) algorithm are consistent with magnetite-ilmenite oxybarometry using the activity model of Ghiorso and Evans (2008) (Crabtree & Lange, 2011; Waters & Lange, 2016). Table 3.1 summarizes the oxybarometric methods we apply and the studies we include. A more detailed discussion of alternative parameterizations for fO_2 can be found in the methods appendix. The compiled dataset can be downloaded as a data library (Cottrell et al., 2021). The dataset is unique in that we aggregate fO_2 data from different studies, different authors, and with different proxies, but we reprocess and quality check the data to facilitate global comparisons. This exercise also identifies which regions and tectonic settings lack direct fO_2 constraints (Figure 3.1).

We first present the Fe-proxy-based fO_2s recorded by rocks from each tectonic setting (ridge, back arc, arc, and plume). We discuss the processes that may perturb these proxies and the extent to which the fO_2 recorded by rock samples is representative of the mantle source. We then compare Fe-based proxies to the inferences that can be drawn from magmatic V concentrations across tectonic settings. Like all elements, the V concentrations of basaltic liquids change as fractional crystallization proceeds, necessitating the normalization of V concentration to another trace element. Although many studies normalize V concentrations to Scandium (Sc), Mallmann and O'Neill (2009) and Laubier et al. (2014) critically evaluate candidate trivalent cations and conclude that the V/Sc ratio does not remain constant as fractionation proceeds. V/Sc begins to rise as MgO falls below 8 wt.%, making this ratio unsuitable to evaluate primitive arc basalts (Laubier et al., 2014). Following Laubier et al. *(2014)* we choose Yb for normalization because it remains constant during crystallization of typical basalts down to < 6 wt.% MgO. We use the compilation of Gale et al. (2013a) for MORB and BABB chemistry, which ensures that samples derive from on-axis locations and that trace element analyses are of high quality. We use the compilation of Turner and Langmuir (2015) for arc basalt chemistry, which ensures that samples derive from arc-front volcanoes and, again, that trace element analyses are of high quality. Following Laubier et al. (2014), we filter these compilations for 6 wt.% < MgO < 12 wt.% to ensure that we are evaluating compositions that represent liquids (not cumulates) and that magnetite has not yet begun to crystallize (V is compatible in magnetite). We only evaluate compositions with Dy/Yb < 2 to avoid residual garnet in the source (Laubier et al., 2014). With these filters in place, we compile trace element data for 1294 MORB and 225 BABB, as well as 317 basalts from 37 arc-front volcanoes. We did not include plume-derived basalts in this comparison because the residual garnet in plume sources complicates interpretation of V/Yb. Yb (and Sc) are highly compatible in garnet, and the relationship between V/Yb (or V/Sc) and fO_2 is poorly defined (Canil, 2002; Davis et al., 2013; Lee et al., 2005).

3.3. RESULTS

Calculated fO_2 for each sample in this study is available in the data library associated with this publication (Cottrell et al., 2021).

3.3.1. Fe-Based Oxybarometry

Mid-Ocean Ridges. Mid-ocean ridges sample Earth's convecting mantle and represent the majority of volcanism on the planet. Both melts and mantle

Table 3.1 Results and Method Summary.

Tectonic setting	δQFM (s)	Lithology	n	Method	Activity-composition models and other method notes	Method error in fO_2 in log units	Notes	Data included
mid-ocean ridge	–0.17 (0.15)	basalt pillow glass	160	XANES	At 1atm. Kress & Carmichael, 1991; parameterization of fO_2 as a function of composition	0.27	Fe oxidation state determined using the Mössbauer calibration of Zhang et al., 2018	Cottrell & Kelley, 2011; Le Voyer et al., 2015 (except the 6 analyses of hydrothermally altered dredge 16D); Birner et al., 2018
mid-ocean ridge	0.19 (0.36)	basalt pillow glass	42	XANES	At 1atm. O'Neill et al., 2018; parameterization of fO_2 as a function of composition	0.52	Fe oxidation state determined using the Mössbauer calibration of Berry et al., 2018	O'Neill et al., 2018
mid-ocean ridge	0.16 (–)	lava	1	mag-ilm pairs	fO_2 at T recorded and 1 atm. Ghiorso & Evans 2008	0.25**	passes Bacon & Hirschmann, 1988, test for equilibrium	Mazzullo & Bence, 1976
mid-ocean ridge	0.31 (0.73)	peridotite	72	sp-oxybarometry	fO_2 at T and 0.6GPa. Mattioli & Wood, 1988; and Wood & Virgo, 1989; with aFe_3O_4 from Sack & Ghiorso, 1991a, 1991b; http://melts.ofm-research.org/CalcForms/index.html; Temperature from spinel-olivine Fe-Mg exchange thermometer of Li et al., 1995	Between about +0.6/–1.0 and ±0.2 depending on spinel $Fe^{3+}/\Sigma Fe$ ratio of spinel (see Methods Appendix and Davis et al., 2017)***	see Davis et al., 2017; and Birner et al. 2017; for discussions of a-X model choices	Bryndzia & Wood, 1990; Birner et al., 2018
back arc basin spreading center	0.22 (0.30)	submarine lava	37	XANES	at 1atm and 1200°C. Kress & Carmichael, 1991	0.27		Kelley & Cottrell, 2009; Brounce et al., 2014
arc front	0.96 (0.39)	basalt glass in olivine-hosted inclusions, basalt pillow glass	119	XANES	at 1atm and 1200°C. Kress & Carmichael, 1991	0.27		Bonnin-Mosbah, 2001; Kelley & Cottrell, 2009; Kelley & Cottrell, 2012; Brounce et al., 2014; Brounce et al., 2016 (data from Gaetani et al., 2012, excluded from average due to oxidative beam damage)
arc front	1.28 (0.64)	volcanics (lavas and tephra)	114	mag-ilm pairs	fO_2 at T recorded and 1 atm. Ghiroso & Evans, 2008	0.25**	passes Bacon & Hirschmann, 1988, test for equilibrium	Carmichael, 1967; Luhr & Carmichael, 1980; Wallace & Carmichael, 1994; Rutherford & Devine, 1996; Mandeville et al., 1996; Luhr, 2000; Coombs & Gardner, 2001; Devine et al., 2003; Costa et al., 2004; Grove et al., 2005; Larsen, 2006; Toothill et al., 2007; Izbekov et al., 2002; Browne et al., 2010; Baggerman & Debari, 2011; Crabtree & Lange, 2011; Stelten & Cooper, 2012; Arce et al., 2013; Waters & Lange, 2013; Howe et al., 2014; Frey & Lange, 2011; Muir et al., 2014; Waters et al., 2015; Grocke et al., 2016; Crabtree & Waters, 2017; Waters & Frey, 2018
arc front	0.96 (0.81)	peridotite xenoliths	47	sp-oxybarometry	fO_2 at T and 0.6GPa. Mattioli & Wood, 1988; and Wood & Virgo, 1989; with aFe_3O_4 from Sack & Ghiorso, 1991a, 1991b; http://melts.ofm-research.org/CalcForms/index.html; Temperature from spinel-olivine Fe-Mg exchange thermometer of Li et al., 1995	Between about +0.6/–1.0 and ±0.2 depending on spinel $Fe^{3+}/\Sigma Fe$ ratio of spinel (see Methods Appendix and Davis et al., 2017)***	see Davis et al., 2017; and Birner et al., 2017; for discussions of a-X model choices	Wood & Virgo, 1989; Canil, 1990; Brandon & Draper, 1996; Parkinson et al., 2003; Bénard et al., 2018

(*continued overleaf*)

Table 3.1 (*Continued*)

Tectonic setting	δQFM (s)	Lithology	n	Method	Activity-composition models and other method notes	Method error in fO_2 in log units	Notes	Data included
forearc	0.22 (0.75)	trench wall peridotite and peridotite xenoliths	64	sp-oxybarometry	fO_2 at T and 0.6GPa. Mattioli & Wood, 1988; and Wood & Virgo, 1989; with aFe_3O_4 from Sack & Ghiorso, 1991a, 1991b; http://melts.ofm-research.org/CalcForms/index.html; Temperature from spinel-olivine Fe-Mg exchange thermometer of Li et al., 1995	Between about +0.6/–1.0 and ±0.2 depending on spinel $Fe^{3+}/\Sigma Fe$ ratio of spinel (see Methods Appendix and Davis et al., 2017)∗∗∗	see Davis et al., 2017; and Birner et al., 2017; for discussions of a-X model choices	Parkinson & Pearce, 1998; Pearce et al., 2000; Birner et al., 2017
plume	0.10∗ (0.71)	basalt pillow glass	334	XANES	at 1atm and 1200°C. Kress & Carmichael, 1991	0.59	Studies using the standard glasses of Cottrell et al., 2009, are recalculated using the Fe3+/Fe2+ ratios reported by Zhang et al., 2018	Brounce et al., 2017; Moussallam et al., 2014; Helz et al., 2017; Moussallam et al., 2016; Shorttle et al., 2015; Hartley et al., 2017; Moussallam et al., 2019
plume	–0.25 (0.55)	lavas	47	mag-ilm pairs	fO_2 at T recorded and 1 atm. Ghiorso & Evans, 2008	0.25∗∗	passes Bacon & Hirschmann, 1988, test for equilibrium	Carmichael, 1967a,b; Anderson & Wright, 1972; Wolfe et al., 1997; Hasse et al., 1997; Gunnarsson et al., 1998; Beier et al., 2006; Genske et al., 2012; Portnyagin et al., 2012
plume	0.82 (1.40) at 0.6 GPa and 0.10 (1.42) at 2.5 GPa	peridotite and pyroxenite xenoliths	143	sp-oxybarometry	fO_2 at T and 0.6GPa. Mattioli & Wood, 1988; and Wood & Virgo, 1989; with aFe_3O_4 from Sack & Ghiorso, 1991a, 1991b; http://melts.ofm-research.org/CalcForms/index.html; Temperature from spinel-olivine Fe-Mg exchange thermometer of Li et al., 1995	Between about +1.2/–2.0 and ±0.4 depending on spinel $Fe^{3+}/\Sigma Fe$ ratio of spinel (see Methods Appendix and Davis et al., 2017)∗∗∗	see Davis et al., 2017; and Birner et al. 2017; for discussions of a-X model choices	Abu El-Rus et al., 2006; Bonadiman et al., 2005; Davis et al., 2017; Grégoire et al., 2000; Hauri & Hart, 1994; Kyser et al., 1981; Neumann, 1991; Neumann et al., 1995; Neumann et al., 2002; Ryabchikov et al. 1995; Sen, 1987; Sen, 1988; Sen & Leeman, 1991; Sen & Presnall, 1986; Tracy, 1980; Wasilewski et al., 2017; Wulff-Pedersen et al. 1996

Note: ∗Authors of these studies infer higher fO_2 for primitive, near primary, melts based on these data: Mauna Kea >QFM 0.6 (Brounce et al., 2017); Kilauea QFM +0.4 to 0.7 (Helz et al., 2017, Moussallam et al., 2016); Iceland ~QFM + 0.4 (Shorttle et al., 2015; Hartley et al., 2017); Erebus ~QFM + 1.4 (Moussallam et al., 2014); Canary Islands ~QFM + 1.0 (Moussallam et al., 2019)

Note: ∗∗Magnetite-Ilmenite oxygen barometery errors reflect the average residual of model calcluations and the calibration dataset: (Ghiroso & Evans [2008] oxygen barometer-derived fO_2 – known fO_2 from calibration dataset), presented in supplemental material of Waters & Lange (2016)

Note: ∗∗∗Uncertainty in fO_2 calculated from spinel oxybarometry is asymmetrical and decreases in magnitude as $Fe^{3+}/\Sigma Fe$ ratio of spinel increases. Spinels that have $Fe^{3+}/\Sigma Fe = 0.05$ have an uncertainty in log fO_2 at the high end listed and those with $Fe^{3+}/\Sigma Fe \geq 0.4$ at the low end. Hotspot residues, except four from Davis et al. (2017), are samples with spinel $Fe^{3+}/\Sigma Fe$ ratios determined without Mössbauer correction standards, which roughly doubles uncertainty compared to corrected analyses (Davis et al., 2017).

lithologies offer opportunities for oxybarometry. We begin with the volcanics.

Early estimates based on wet chemistry and magnetite–ilmenite pairs indicated that mid-ocean ridge basalts (MORBs) record fO_2s similar to QFM (Carmichael & Ghiorso, 1986; Haggerty, 1976). However, upon reexamining data from the literature compiled by Haggerty (1976), we found only one sample with multiple pairs of magnetite and ilmenite in equilibrium at magmatic temperatures according to Bacon and Hirschmann (1988), and that sample (15.6m cooling unit from DSDP Leg34: site 319A) records QFM+0.16 (±0.1) at 1232 (±37)°C (Mazzullo & Bence, 1976). Subsequent wet chemical work found that MORBs record fO_2s low enough to suggest graphite is a stable phase in the MORB source (i.e., ~QFM-1, Christie et al., 1986), but more recent wet-chemical work and Fe K-edge XANES analyses have revised average MORB fO_2 estimates back upwards to QFM (Bezos & Humler, 2005; Cottrell & Kelley, 2011; O'Neill et al., 2018; Zhang et al., 2018). Five recent studies determine $Fe^{3+}/\Sigma Fe$ ratios spectroscopically by XANES to determine the fO_2 of average MORB

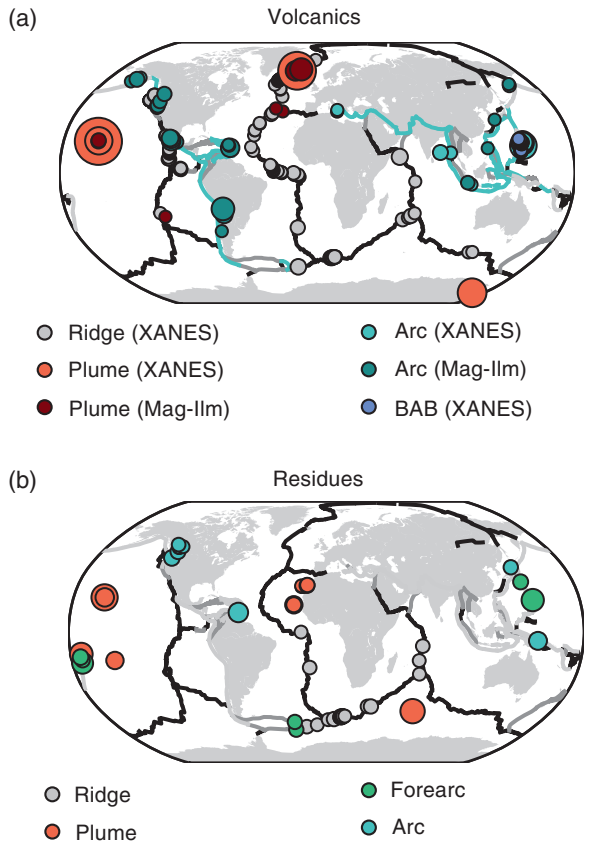

Figure 3.1 Locations of samples compiled in this study as a function of tectonic setting, lithology, and methodology. Symbol size scales linearly with the number of samples at a given locality.

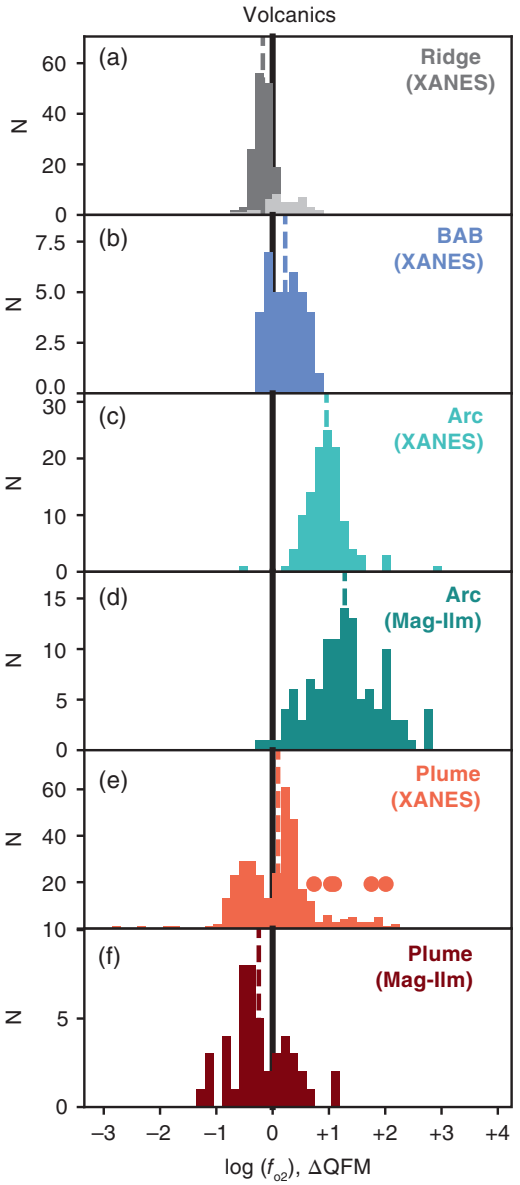

Figure 3.2 Distribution of fO_2 recorded by volcanics globally in different tectonic settings and by multiple methods of oxybarometry. We have recalculated the fO_2 recorded by each sample based on the reported chemical analyses except for the separate light gray dataset in panel (a), which are the observations as reported by O'Neill et al. (2018). The O'Neill et al. (2018) dataset was collected using a different set of primary standards, as described in our methods appendix. Vertical, dashed lines reflect calculated average values of fO_2. Note that volcanics in (e) include plume-affected ridge segments, which cause them to record bimodal fO_2; the fO_2s inferred for primitive plume magmas are higher than the average and we represent each plume's primitive magma fO_2 as a filled orange circle (as reported by those authors). See Table 3.1 and text for details.

(Fig. 3.1, Fig. 3.2a) (Birner et al., 2018; Cottrell & Kelley, 2011; Le Voyer et al., 2015; O'Neill et al., 2018; Zhang et al., 2018). Determinations for 166 MORB glasses that use the calibration of Zhang et al. (2018) find a narrow distribution around QFM –0.17±0.15 (all uncertainty is 1 standard deviation [σ] unless otherwise noted). Determinations for 42 MORB using the calibration of Berry et al. (2018) by O'Neill et al. (2018) return a mean of QFM +0.19 ±0.36. It is notable that O'Neill et al. (2018)'s corresponding $Fe^{3+}/\Sigma Fe$ ratios for average MORB are *lower* by ~0.04 than those from the global survey of Zhang et al. (2018), despite their equation to higher fO_2. The difference stems from O'Neill et al. (2018)'s application of a new compositional parameterization of fO_2, which we choose not to apply in this study (see Methods Appendix for a description and assessment of parameterizations). The important point for our purpose here is that, regardless of the value of the $Fe^{3+}/\Sigma Fe$ ratio of natural MORB, the Fe-XANES spectra of natural MORB glasses resemble the spectra of experimental MORB-composition glasses equilibrated at fO_2 similar to the QFM buffer (see Methods Appendix, Fig. S1), and there is general agreement among all recent spectroscopic studies that MORB glasses record QFM. The fO_2s recorded by average MORBs (7.58 wt.% MgO, Gale et al., 2013b) will be maxima with respect to the fO_2 of the mantle from which they derive, because Fe^{3+} is moderately incompatible during low-pressure fractional crystallization and average MORBs are not primary melts of the mantle ($Fe^{3+}/\Sigma Fe$ ratios increase by 0.03 as MgO falls from 10 to 5 wt.%; Cottrell & Kelley, 2011).

Oxybarometry of mid-ocean ridge peridotites has only been investigated in two studies (Birner et al., 2018 and Bryndzia & Wood, 1990) and in a handful of localities (Fig. 3.1). Global ridge peridotites record fO_2 = QFM +0.31 (±0.73), but we note that more than half of these data derive from a single ridge segment (Fig. 3.1, Fig. 3.3a). Birner et al. (2018) found that n=41 peridotites dredged from the Southwest Indian Ridge (SWIR) record QFM +0.61 (±0.63) at 0.6 GPa and the closure temperature of olivine-spinel exchange. This is significantly higher than the fO_2 recorded by basalts on the same segment (p-value < 0.01); however, the discrepancy disappears once the peridotites' conditions of last equilibration with basalt are considered (Birner et al., 2018). The method of projecting peridotite fO_2 to the PTX conditions of last equilibration with basalt considers three sub-solidus reactions that may alter the fO_2 recorded by the rock: Mg–Fe exchange between olivine and spinel, Al–Cr exchange between spinel and orthopyroxene, and a Tschermak reaction that produces spinel at the expense of olivine and Al-rich orthopyroxene during cooling. Although a dearth of knowledge as to ferric iron partitioning behavior between spinel and pyroxenes during cooling leads to

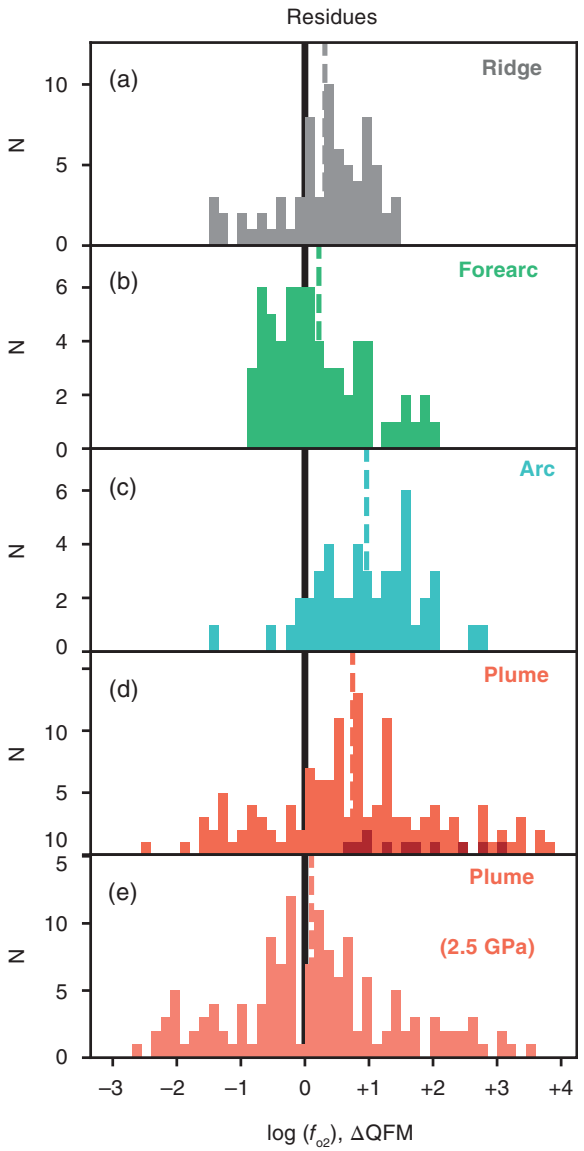

Figure 3.3 Distribution of fO_2 recorded by mantle lithologies (peridotites and olivine-orthopyroxene-spinel-bearing pyroxenites) globally in different tectonic settings. We have recalculated the fO_2 recorded by each sample at 0.6 GPa (2.5 GPa in [e]) and temperature recorded by spinel-olivine thermometry using the methodology of Birner et al. (2018) and Davis et al. (2017) based on the reported chemical analyses. All samples are peridotites except for (d) where the overlain histogram in red are pyroxenites. We caution against overinterpreting the wide range of xenolith fO_2s recovered at plumes due to (i) the near absence of samples from this setting characterized using Mössbauer-characterized spinel standards or Mössbauer spectroscopy; (ii) uncertainty in the barometry and metamorphic history of these samples (which will alter the fO_2 they record); and (iii) limited data by which we may judge the extent to which these lithospheric xenoliths record ridge versus plume fO_2.

significant uncertainty in the magnitude of projection (±0.5 log units, Birner et al., 2018), the direction of the model is to decrease recorded peridotite fO_2 values when projecting back to high temperature-pressure source conditions. This projection thus brings peridotite fO_2 values into closer agreement with basalt fO_2 values, suggesting that fO_2 values recorded by peridotites, without these corrections, may systematically overestimate the redox conditions of MORB-source mantle (Birner et al., 2018).

We highlight that peridotites along SWIR record five times greater range in fO_2 when compared to basalts dredged from the same segment. On the global scale, Bryndzia and Wood (1990) investigated the fO_2 of 35 ridge peridotites from 12 localities. When filtered to exclude four samples from two anomalous locations (the subaerial St. Paul's Rocks and the tectonically complex Mid-Cayman Rise), and recalculated according to the methods presented here, this sample set records fO_2 of QFM -0.08 ±0.68 and spans a range of nearly 2.5 orders of magnitude in fO_2 (Birner et al., 2018). When comparing Fig. 3.2a and 3.3a, we observe that global mid-ocean ridge volcanics display low variance relative to ridge peridotites. These limited data suggest that basalts may homogenize kilometer-scale redox heterogeneity in the upper mantle (Birner et al., 2018). Globally, ridge peridotites calculated at 0.6 GPa and the temperature of olivine-spinel closure record average fO_2s about half a log unit higher than basalts calculated at 1 bar and 1200 °C. Because we have not attempted here to account for subsolidus processes in the peridotites globally, comparisons between the two distributions should not be overinterpreted. A more comprehensive global peridotite dataset is required to evaluate the response of mantle residues to melt extraction and subsolidus re-equilibration.

Arcs and Back Arcs. Subduction influences the composition of mantle melts and arc volcanics, generating continental crust in the process (e.g., Elliott et al., 1997; Gill, 1981; Grove et al., 2012; Kelemen et al., 2003; Kelemen et al., 2007; Osborn, 1959; Plank & Langmuir, 1988; Stolper & Newman, 1994; Turner & Langmuir, 2015; Zimmer et al., 2010). Both melts and mantle lithologies offer opportunities for oxybarometry. We begin with the volcanics.

Seminal contributions by Carmichael (1991) and Frost and Lindsley (1992) surveyed the fO_2s recorded by arc rocks using wet-chemistry and magnetite-ilmenite pairs, respectively, and found that arc rocks record fO_2s up to several orders of magnitude higher than MORBs. Our compilation of 5 XANES spectroscopic studies (n=119 samples, Figure 3.2c) of olivine-hosted melt inclusions and submarine pillow glasses shows that arc basalts record, on average, QFM +0.96 (±0.39). One set of outliers from Cerro Negro record QFM +4.75 (±0.40) (Gaetani et al., 2012), but spectra from these hydrous samples have suffered from radiation-induced beam damage (Cottrell et al., 2018, Gaetani, pers. comm.) and are not included in our statistical analysis. Nearly 90% of samples with XANES measurements erupted through the thin crust (~25 km, Takahashi et al., 2007) of the active Mariana arc front (Fig. 3.1a), and thus there is significant location bias in this dataset.

Globally, magnetite–ilmenite pairs, from 114 arc lavas sampling 11 different arcs, record QFM +1.28 (±0.64) (Figure 3.2d; see methods appendix and the online data library associated with this contribution, Cottrell et al., 2021, for citations). These samples contain Fe–Ti oxides with compositions that record a range of temperatures (700–1085 °C), span a wide range of compositions (basaltic andesite to rhyolite) but are predominantly dacitic, and erupt through crust ranging from 25 to 66km thick.

The mean fO_2 recorded by olivine-hosted melt inclusions and submarine arc-front glasses (ΔQFM = 0.96 ±0.39, n=119) is slightly lower than that recorded by magnetite-ilmenite pairs (ΔQFM = 1.28±0.64 n=114) at the 95% confidence level ($t_{statistic}$ = 4.6, $t_{critical}$ = 2.0, degrees of freedom [DF] = 186, p-value < 0.001). (When we compare distribution means in this contribution, we will always apply a two-sample student's t-test with α= 0.05 [Krzywinski & Altman, 2013] for samples of unequal variance.) We caution that the datasets are not directly comparable because of the limited geographic distribution of the melt inclusion and submarine glass dataset; because there are no samples in common between the two distributions; and because the melt inclusions may reflect magma compositions that precede magnetite and ilmenite saturation. Thus, to first order, our global result is not inconsistent with the results of Waters and Lange (2016) and Crabtree and Lange (2011) who found congruence when they compared magnetite-ilmenite oxybarometry to wet-chemical titration on the same suite of very fresh aphyric lavas.

A more direct comparison can be made between the olivine-hosted melt inclusions and submarine glasses erupted along the active Mariana Arc, and back arc basin (BAB) glasses erupted at depth along the associated back arc spreading center: the Mariana Trough. Both datasets apply the same method (XANES) to arrive at fO_2 estimates, and both sample suites comprise basaltic to basaltic andesite glasses representing similar stages of differentiation in thin crust (similar MgO). The Mariana arc front samples record fO_2s that are on average 0.73 log units higher than the Mariana trough samples (Mariana arc: QFM+0.95±0.36 for n = 107 vs Mariana trough: QFM+0.22±0.30 for n=37, respectively) (Brounce et al., 2014; Kelley & Cottrell, 2009).

Another direct comparison can be made between submarine basalts in ridge (MORB) and BAB tectonic settings. Here we find that BAB from the Mariana trough (n=37) record significantly higher fO_2s than MORB

globally (n=160) by 0.4 log units ($t_{statistic}$ = 7.8, $t_{critical}$ = 2.0, degrees of freedom [df] = 41, p-value << 0.001). This comparison is particularly germane for inferring the effect of subduction on mantle fO_2 because submarine back-arc ridges and mid-ocean ridges are tectonically similar and differences in their melt chemistry can be largely attributed to the influence of subduction (Stolper & Newman, 1994). As indices of subduction influence in Mariana trough lavas go from negligible to significant (e.g., as H_2O contents and the ratios of fluid mobile to fluid immobile incompatible trace elements increase), $Fe^{3+}/\Sigma Fe$ ratios (and fO_2s) also increase (Brounce et al., 2014; Kelley & Cottrell, 2009, 2012). In the Marianas, volcanics erupted over the course of the arc's maturation also record increasing fO_2 with increasing subduction influence. Modern arc tholeiites record similar fO_2s to the boninites that erupted during the early stages of slab influence on the mantle wedge; and both lithologies are more oxidized than the forearc basalts that tapped the mantle prior to slab influence (Brounce et al., 2021; Brounce et al., 2015). The volatile and trace element signals of subduction appear intimately tied to elevated fO_2s in space and in time.

Mantle lithologies recovered from arc settings comprise primarily forearc and arc peridotites. Forearc peridotites are exposed on trench walls and may sample ancient lithospheric mantle (Parkinson & Pearce, 1998), mantle wedge metamorphosed by the subducting slab (Fryer et al., 1985), or processes associated with subduction initiation (Birner et al., 2017). In comparison, arc peridotites rapidly ascend to the surface as xenoliths encased within their basaltic hosts at arc front volcanoes. The mean fO_2 recorded by forearc peridotites is statistically indistinguishable from the mean fO_2 recorded by ridge peridotites ($t_{statistic}$ = 0.73, $t_{critical}$ = 2, df = 131, p-value = 0.47) (Fig. 3.3). As discussed by Birner et al. (2017), this result contrasts with Parkinson and Pearce (1998)'s study of forearc peridotites from the Izu-Bonin subduction zone, primarily because we apply the spinel activity model of Sack and Ghiorso (1991) instead of Nell and Wood (1991). Yet, consistent with Parkinson and Pearce (1998), Birner et al. (2017) show that peridotites that have interacted with slab-influenced melts do yield elevated fO_2. This influence is additionally evident in the distribution of fO_2 recorded by arc xenoliths from five studies (Table 3.1), which lies significantly higher, by 0.65 log units, than ridge peridotites (t_{stat} = 4.4, t_{crit} = 2.0, df = 90, p-value << 0.001) or forearc peridotites. Another unique characteristic of sub-arc peridotites is the extended range of melt extraction they record. Spinel Cr#, commonly taken as a proxy for melt extraction, extends to much higher values (> 60) in sub-arc peridotites than in ridge peridotites. This extended range of melt extraction may provide an opportunity to investigate the relationship between extent of melting and fO_2. For example, Benard et al. (2018b) found a weak positive correlation (p-value > 0.06) between fO_2 and modal orthopyroxene, which they interpreted as evidence of fO_2 falling with melt extraction; however, the positive correlation between spinel Cr# and fO_2 in these same samples suggests the relationship between fO_2 and melt extraction may be more complicated. No correlation exists between fO_2 and orthopyroxene mode or spinel Cr# in the Tonga peridotites of Birner et al. (2017). More work is needed to better constrain the effects on fO_2 of extracting melt from the mantle.

Plumes. Mantle plumes are thermal upwellings that impinge on the lithosphere (French & Romanowicz, 2015; Montelli et al., 2006; Sleep, 1992). Capable of generating low degree mantle melts that more ably sample mantle heterogeneity, mantle plumes can produce ocean island basalts (OIB) (Dasgupta et al.; McKenzie & Onions, 1983; Stracke et al., 2005) and xenoliths wrenched from the lithospheric mantle (Frey & Roden, 1987). Both melts and xenoliths at ocean islands offer opportunities for oxybarometry; however, it remains challenging to interpret the relationship between lithospheric mantle peridotites and OIB. We begin with the volcanics.

Melt inclusions and submarine basalts erupting at and around the mantle plumes of Hawaii, Erebus, Iceland, and the Canary Islands record, on average, QFM +0.1 (7 XANES spectroscopic studies with n= 334 samples; Table 3.1, Fig. 3.2e). The Fe- XANES-based fO_2 in this case is higher than the record of magnetite–ilmenite pairs (n=47) by 0.35 log units ($t_{statistic}$ = 3.8, $t_{critical}$ = 2, df = 69, p-value = 0.003); however, we emphasize that these datasets have no samples in common. There is no meaningful difference between the fO_2s recorded by OIBs and MORBs. In the case of OIB volcanics, most XANES studies have either interrogated a geographic gradient in fO_2 (e.g., Shorttle et al., 2015) or the effect of differentiation (crystallization and degassing) on fO_2 (e.g. Brounce et al., 2017; Helz et al., 2017; Moussallam et al., 2016; Moussallam et al., 2014). We therefore observe a bimodal distribution of fO_2 recorded by plume-affected glasses (Fig. 3.2e). Glasses erupted along mid-ocean ridges that approach plumes, and glasses affected by degassing, record lower fO_2, while primitive and relatively undegassed melt inclusions record higher fO_2 (Fig. 3.2e, and see discussion). The authors of the detailed studies that have interrogated the fO_2 of plumes and plume-affected ridges have inferred plume mantle source fO_2s anywhere from 0.4 to 2 log units higher than the average fO_2 recorded by the volcanics (filled circles in Figure 3.2e). In all cases, the authors have suggested that the mantle sources of these OIBs are more oxidized than those of MORB, and that this may be due to incorporation of recycled components (e.g. Brounce et al., 2017; Moussallam

et al., 2019; Helz et al., 2017; Moussallam et al., 2016; Moussallam et al., 2014; Shorttle et al., 2015). Investigators have drawn such inferences by projecting the glass $Fe^{3+}/\Sigma Fe$ ratios along compositional trends (e.g., to more primitive, less degassed, and more enriched compositions) or geographic trends (e.g., along a ridge toward a plume). We discuss some of these projections in greater detail in Section 3.4.1.1.

We have additionally compiled data from 13 studies to calculate the fO_2 of 143 ocean island xenoliths. Unlike all of the ridge peridotites and most of the arc peridotites, none of the published spinel compositions, save for Davis et al. (2017), were obtained using spinel standards with $Fe^{3+}/\Sigma Fe$ ratios independently characterized. Without using standards to correct spinel Fe3+/ΣFe ratios, uncertainties in log fO_2 are roughly double those of samples calculated from corrected spinel $Fe^{3+}/\Sigma Fe$ ratios (Davis et al., 2017, see Methods Appendix and Table 3.1). Despite, or because of, this limitation, we see that ocean island xenoliths record a wide range of fO_2, from QFM –2 to nearly QFM +4 with a mean equal to QFM +0.82 (±1.40). This is a much broader range, extending to lower fO_2, than compiled by Ballhaus (1993); the mean is within error of that compiled by Mallmann and O'Neill (2007), though again the variance is greater in the present compilation. Of the 143 xenoliths compiled here, 11 were identified by the original authors as pyroxenites (Sen, 1987; Tracy, 1980) which record a more oxidized mean fO_2 of QFM +1.44 (±0.63) than the whole set of OIB xenoliths (see red histogram overlain on Fig. 3.3d). The range of fO_2 recorded by OIB lavas falls within the range recorded by ocean island xenoliths; however, we cannot draw a genetic relationship between all lithospheric mantle xenoliths and the mantle melts that exhume them at plumes (compare Fig. 3.2e to 3.3d). Presumably, many of these xenoliths represent lithospheric mantle that has experienced limited chemical interaction with plume-derived melts. Others are likely products of melt-rock reaction between lithospheric peridotite and plume-generated melts. The pyroxenite xenoliths were especially likely to have been derived in this way (e.g., Sen & Leeman, 1991), but it is unclear how many of the peridotites were also influenced by plume-sourced melts. There is another caveat; we do not know the equilibration pressure at the closure temperature of these plume xenoliths. At ridges, we can reasonably infer pressure from peridotite thermometry because geothermal gradients are reasonably well-characterized. That is not the case in plume settings, where thermal gradients are radial as well as vertical (e.g., Farnetani & Hofmann, 2010). In Figure 3.3e we demonstrate how equilibration at 2.5 GPa, instead of 0.6 GPa, would shift fO_2 down by two thirds of a log unit. This illustrates our community's need for better peridotite mineral barometry.

We venture that a more appropriate comparison might be drawn between peridotitic ocean island xenoliths and ridge peridotites. Both may initiate as residues of melting at ridges, with the former transiting and cooling prior to interacting with a mantle plume. The range of fO_2s recorded by ocean island xenoliths encompasses the range of ridge peridotites but skews to higher fO_2s by 0.37 log units if we hold pressure constant at 0.6 GPa ($t_{stat} = 2.6$, $t_{crit} = 2.0$, df = 211, p-value = 0.01). Notably, spinel-olivine Fe-Mg exchange (Li et al., 1995) records higher temperatures in the ocean island xenoliths than in the ridge peridotites. This difference in temperature could be the result of heating of the oceanic lithosphere beneath oceanic islands by the plume (Ballhaus, 1993), or it could result from exhumation of these xenoliths from greater depths than the depth of last equilibration experienced by ridge peridotites. In the former case, temperature-dependent exchange reactions suggest that a mantle parcel preserving a record of hotter conditions should record lower fO_2 than a parcel at the same pressure that records cooler conditions (Birner et al., 2018). Consideration of these subsolidus reactions would thus predict ocean island xenoliths to be more reduced than ridge peridotites, in contrast to what we observe. If this interpretation is correct, then the difference in fO_2 between ridge peridotites and OIB xenolith source mantle prior to plume heating is even greater than the 0.6 GPa plots in Figure 3.3 suggest, perhaps driven by the interaction of some of these xenoliths with oxidized plume melts. In the latter case, changes in fO_2 due to changes in pressure would additionally have to be accounted for to make a direct comparison between ridge peridotites and OIB xenoliths. If no changes in mineral composition or mode are considered, the lower average fO_2 calculated assuming a higher pressure of equilibration (Fig. 3.3) suggests that if OIB xenoliths do generally sample deeper portions of the lithosphere than ridge peridotite, then average fO_2 of the two are comparable. While exchange reactions and modal changes during ascension and cooling may complicate this relationship, at this time, the data do not suggest that xenoliths recovered from plumes significantly differ in their fO_2 compared to peridotites recovered in the ridge setting. Constraints on pressure and effects of temperature on the fO_2 recorded by peridotites below their solidus remain poorly understood, and further work is needed to clarify the fO_2 signature of xenoliths entrained within plume lavas.

3.3.2. V/Yb Concentrations

V/Yb ratios range from 17–195 in MORB, 60–238 for BABB, and 65–422 in arcs (excluding one arc basalt with a ratio of > 800). We find average V/Yb concentrations in each tectonic setting that are all statistically distinct (p-values <<< 0.001) with V/Yb of MORB (93 ±17)

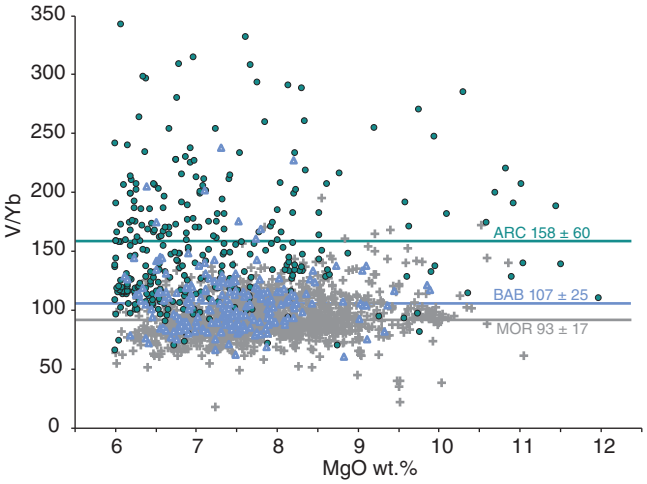

Figure 3.4 V/Yb ratios of ridge (gray "+" symbols, Gale et al., 2013), back-arc (blue triangles, Gale et al., 2013), and arc lavas (teal circles, Turner & Langmuir, 2015) as a function of weight percent MgO. We filtered each published data compilation for 6 wt.% < MgO < 12 wt.% and for Dy/Yb < 2 (Laubier et al., 2014). See text for details.

< BABB (107 ±25) < arcs (158 ±60). We illustrate this in Figure 3.4 with a plot of V/Yb ratios against MgO concentrations in ridge, back-arc, and arc settings. Translating trace element ratios measured in glass (magmatic liquid) to the oxygen fugacity of the source rock (residue) depends on having accurate, composition-dependent, mineral-melt partition coefficients, an accurate knowledge of the source composition, and an accurate melting model (e.g., Canil, 1997; Lee et al., 2003; Lee et al., 2005; Mallmann & O'Neill, 2009; Mallmann et al., 2019). Mallmann and O'Neill (2013), Nicklas et al. (2019), Mallmann et al. (2019), Bucholz and Kelemen (2019), and others have discussed the difficulty in translating V/Sc ratios or olivine-melt partition coefficients into source fO_2s. For example, the fO_2 of modern MORB, or Archean mantle, based on V partitioning is up to a log unit *higher* than that implied by modern MORB $Fe^{3+}/\Sigma Fe$ ratios (Mallmann and O'Neill, 2013; Nicklas et al., 2019). For these reasons, we do not calculate fO_2 for each tectonic setting based on the V/Yb ratio, but simply infer the relative oxygen fugacity of each tectonic setting based on the premise that basalt V/Yb will rise with the fO_2 of the mantle source that generated the basalt. Under these assumptions, it is clear that fO_2 ridges < fO_2 back arcs < fO_2 arcs.

3.4. DISCUSSION

Our compilation and reprocessing of analytical data from the literature yields a synoptic picture of the fO_2s recorded by volcanic and mantle rocks across tectonic settings. Some three decades have passed since the seminal compilations from last century (e.g., Ballhaus et al., 1991; Carmichael, 1991; Christie et al., 1986; Frost & Lindsley, 1992; Wood et al., 1990). The volume of data and geographic coverage have increased tremendously and the analytical techniques and activity models have evolved; however, a key finding from those studies remains robust today. Volcanic and mantle rocks from arc settings record significantly higher fO_2 than those from ridges. Recycling of oceanic crust and lithosphere back into the Earth at subduction zones generates arc volcanics and related mantle lithologies that record higher fO_2 relative to those recovered from ridges. Additional work, particularly in forearc and back-arc settings, support this observation by showing that fO_2 becomes elevated in proportion to the rock's subduction affinity (Benard et al., 2018; Birner et al., 2017; Brounce et al., 2014; Brounce et al., 2021; Brounce et al., 2015; Kelley & Cottrell, 2009; 2012; Parkinson & Arculus, 1999). This remains true for the back-arc basin basalts erupted at pressures > 200 bar and through a comparable crustal column to normal MORB. Moreover, in both the ridge and arc settings, melts (lavas and tephras) and mantle (peridotites and pyroxenites) both record an offset in oxygen fugacity of similar magnitude between the two settings. While these observations are robust, the mechanism by which subduction generates more oxidized lavas and associated mantle lithologies remains a matter of debate and is beyond the scope of this contribution to review (e.g., Andreani et al., 2013; Benard et al., 2018; Canil & Fellows, 2017; Carmichael, 1991; Chin et al., 2018; Debret et al., 2014; Evans, this volume; Farner & Lee, 2017; Foden et al., 2018; Gaillard et al., 2015; Kelley & Cottrell, 2009; Lecuyer & Ricard, 1999; Lee et al., 2005; Mungall, 2002; Nebel et al., 2015; Parkinson & Arculus, 1999; Tang et al., 2018; Tollan & Hermann, 2019; Williams et al., 2004; Wood et al., 1990).

3.4.1. Linking the fO_2 of Volcanics and Mantle Lithologies

Linking magmatic fO_2 to melt residue fO_2 and, ultimately, to the fO_2 of the subsolidus convecting mantle presents a grand challenge to the fields of petrology, experimental petrology, and modeling. When the mantle first begins to melt at infinitesimally small melt fractions, the composition of residual silicate phases will not change significantly, and the fO_2 of the unmelted, solid mantle source will impose fO_2 on low degree partial melts (whether silicate melts or carbonated silicate melts), and set the melt's $Fe^{3+}/\Sigma Fe$ ratio. However, at some point during adiabatic ascent, the melt fraction will grow to an extent that the composition of the solid phases are themselves modified, and the fO_2 of the assemblage

(solid + melt) changes. Examples of anticipated changes during melting that could affect fO_2 include the exhaustion of reduced carbon or sulfur phases from the solid assemblage (Lee et al., 2012; Stagno et al., 2013), and an increase of the $Fe^{3+}/\Sigma Fe$ ratio of spinel resulting from Al/Fe^{3+} exchange with the melt that favors concentrating Fe^{3+} in the spinel (Ballhaus et al., 1991; Davis & Cottrell, 2018). At this point, the fO_2 of the mantle will change in ways that experiments and models have not yet elucidated. Indeed, experiments that investigate fO_2 as a variable in the context of partially melting the mantle are nascent (Ballhaus et al., 1991; Davis & Cottrell, 2018; Sorbadere et al., 2018), and stand as a challenge for the future (see Section 3.5). However, once melt and residue separate, melt fO_2 changes little relative to the QFM buffer during volatile-undersaturated adiabatic ascent (Kress & Carmichael, 1991). Thus, at ridges, near primary basaltic melts should serve as accurate proxies for average mantle source conditions (e.g., Carmichael, 1991); however, such accuracy may not extend to mantle rocks, and volcanic rocks from other settings.

Once melts become volatile saturated or begin to undergo assimilation-fractional crystallization processes within the crust, the relationship between mantle source and magmatic fO_2 may become more tenuous. Here we briefly review processes that may modify melt fO_2 signal from source to surface: degassing and crystal fractionation within thick crust.

Degassing. Observational studies that have investigated the relationship between degassing and magmatic fO_2 have thus far observed reduction of melt $Fe^{3+}/\Sigma Fe$ ratios in response to degassing. For example, numerous XANES studies on natural glasses have captured the potential for sulfur degassing to reduce melt $Fe^{3+}/\Sigma Fe$ ratios (Brounce et al., 2014; Brounce et al., 2017; Hartley et al., 2017; Helz et al., 2017; Kelley & Cottrell, 2012; Moussallam et al., 2016; Moussallam et al., 2014; Moussallam et al.; Shorttle et al., 2015). In order to gain further insight into the effect of C–O–H–S degassing on magmatic fO_2, we present results from the gas-melt equilibrium model D-Compress of Burgisser et al. (2015) (see Methods Appendix). Detailed explanations of how D-Compress treats fO_2 during degassing can be found in Burgisser et al. (2015), Moussallam et al. (2016), and Brounce et al. (2017). A general feature of the model output is a prediction of modest changes in fO_2 (< 0.2 log units), both positive and negative, as degassing proceeds until pressures fall below ~250 bar, at which point fO_2 falls sharply in all tectonic settings (Fig. 3.5). D-Compress therefore predicts that the fO_2 of MORB is negligibly affected by degassing (Fig. 3.5, gray line) owing to the fact that MORBs erupt at pressures greater than 200 bar and the dominant degassing volatile is, which has limited

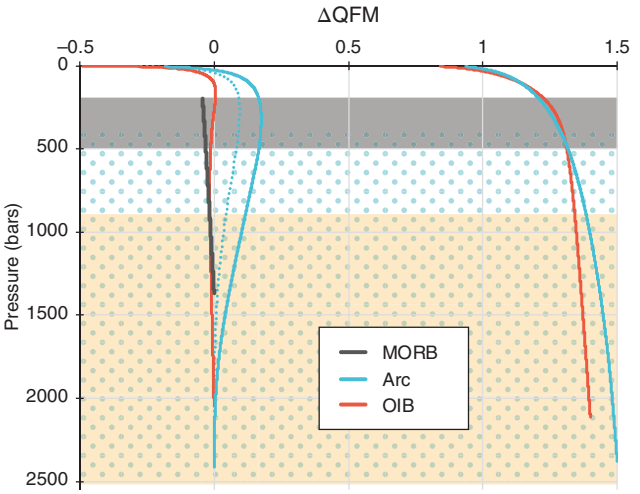

Figure 3.5 Progressive degassing of a C–O–H–S vapor in ridge, arc, and plume settings using the gas-melt equilibrium model D-Compress of Burgisser et al. (2015). For the model run shown by the dashed blue curve, we have set the solubility of H2 in silicate melt to zero; this assumption creates no resolvable difference for any of the other curves shown. For DCompress model details, see the Methods Appendix. Model runs marked OIB, Arc, and MORB are intended to mimic the degassing trajectories of typical magmas from each setting (see methods appendix for details). The OIB and arc scenarios were each run at QFM and near QFM +1.5 to demonstrate the impact of initial fO_2 on degassing trajectory. Orange shaded field shows estimated entrapment pressures for olivine-hosted melt inclusions in OIB based on water and CO_2 concentrations (Tucker et al., 2019). Teal stippled field shows minimum estimated entrapment pressures for olivine-hosted melt inclusions considering water concentrations alone (Plank et al., 2013), which will underestimate typical entrapment pressures. Gray shaded field shows eruption pressures for MORB, which are constrained by ridge depth.

power to shift magmatic fO_2 so long as the MORB source is more oxidized than graphite saturation (Cottrell and Kelley, 2011). Degassing-fO_2 pathways at arcs and subaerial plume volcanoes have greater potential to shift fO_2 because lavas and tephras can degas to 1 atmosphere total pressure. However, melt inclusions may be trapped at nearly any point along the degassing pathway, which may spare some arc and plume sample sets from recording strong modification. Typical water contents of arc melt inclusions yield a conservative estimate of entrapment pressures of 400–3000 bar (Plank et al., 2013). At these entrapment pressures, arc magmas with typical volatile concentrations may be slightly more or less oxidized, but within ~0.2 log units of their source, depending on their initial fO_2 (Fig. 3.5). The fact that arc melt inclusions become progressively reduced during degassing (e.g., Helz et al., 2017; Kelley & Cottrell, 2012; Moussallam et al., 2014; Moussallam et al., 2019) strongly indicates that

the arc source is significantly more oxidized than MORB (compare teal arc degassing pathways initiated at QFM vs QFM +1.5 in Figure 3.5).

The much higher ratios of sulfur to water in undegassed OIB magmas lead to a larger magnitude of reduction as degassing proceeds in OIB settings compared to arc settings, because the reducing effects of degassing ~2000 ppm S are not as strongly offset by the slightly oxidizing effects of degassing H_2O, as is the case for H_2O-rich arc magmas (Fig. 3.5, orange lines). The model predictions in Fig. 3.5 that link degassing to reduction are consistent with observations of natural glass and melt inclusion suites, as reviewed above, and implies that the fO_2 recorded by plume-source glasses is typically a minimum (Brounce et al., 2017; Helz et al., 2017; Moussallam et al., 2019). Corroborating evidence is found when we compare the more primitive and less degassed plume glasses (orange circles, Fig. 3.2e) to magnetite–ilmenite oxybarometry in plume lavas (Fig. 3.2f). The latter record lower fO_2 on average, and we speculate that this may reflect magnetite and ilmenite crystallization further along the liquid line of descent, after significant degassing. Further, if fractional crystallization acts to oxidize iron in typical plume lavas, its effect is either counterbalanced by degassing or is not on display here as we compare these two proxies. The caveat is that these are global compilations; Fig. 3.2e and 3.2f do not have samples in common, and we need targeted studies to untangle these competing effects.

If we look to the mantle for further insights about plume fO_2, we find additional evidence that plumes may be oxidized, but the story remains nuanced. Pyroxenite xenoliths from OIB localities have been interpreted as the products of extensive refertilization of the lithosphere by plume-derived melts (Sen & Leeman, 1991). The relatively oxidized fO_2 recorded by these pyroxenite xenoliths provides further evidence that OIB source regions are more oxidized than the MORB source (Figure 3.3d). The opportunity to investigate the $Fe^{3+}/\Sigma Fe$ ratios of submarine and melt inclusion suites from arcs and plumes holds great future promise for reconstructing primitive melt compositions from partially degassed samples.

Crystal Fractionation. Cottrell and Kelley (2011) and numerous studies since (Birner et al., 2018; O'Neill et al., 2018; Shorttle et al., 2015), have shown how $Fe^{3+}/\Sigma Fe$ ratios increase during low-pressure crystal fractionation by a few percent, and that the fO_2 of MORB glass spans a smaller range of fO_2 (e.g., Fig. 3.2a) than indicated by wet-chemistry. However, extensive crystal fractionation and crustal assimilation are commonly observed in magmas that transit thick arc crust, and this has been invoked to shift magmatic fO_2 away from its mantle source (e.g., Chin et al., 2018; Grocke et al., 2016; Lee et al., 2005; Tang et al., 2018). The dearth of fO_2 studies on the rare basalts and olivine-hosted melt inclusions that transit the continental crust poses a challenge to the community. Insights can be gleaned, however, from extensive analytical work on magnetite–ilmenite pairs in more evolved arc rocks. In the arc crust, we observe that magnetite–ilmenite only precipitate once primary magmas have fractionated significant quantities of olivine and clinopyroxene (which remove Fe^{2+} from the melt), and magnetite–ilmenite pairs in arc lavas record slightly higher fO_2s than primitive arc glasses, in accordance with this expectation (see Results, Table 3.1, and Fig. 3.2). Within the BABB suite, silica and fO_2 do covary, although this relationship is demonstrably unrelated to crystal fractionation (Brounce et al., 2014). SiO_2 and fO_2 covary because of two independent phenomena: melting more hydrous mantle yields primary magmas with higher SiO_2 concentrations (Kushiro, 1972) and melting mantle with more subduction influence yields primary magmas with higher fO_2s and also more water (Kelley & Cottrell, 2009).

Figure 3.6 shows all of the volcanic data we have compiled as a function of both crustal thickness (from 7 to nearly 70 kilometers), SiO_2 concentration (a proxy for crystal fractionation, ranging from ~45 to > 75 wt.%), and SiO_2/Alkali ratios. We observe that magmas record fO_2s in excess of ~QFM +1 only when the crust is thicker than that found in the ridge setting. However, from volcanics erupted through ~25 km of oceanic crust to volcanics erupted through nearly 70 km of continental crust, we observe no global correlation between crustal thickness and fO_2. Neither do we observe a correlation between fO_2 and silica content or SiO_2/alkalis, within or among arcs. Figure 3.6 demonstrates that, to first order and on average, there is no simple relationship amongst the variables of crustal thickness, differentiation, and oxygen fugacity. Thus, while the relative influence of slab characteristics, the mantle wedge, and differentiation within the overlying crust on the geochemistry of arcs in the broadest sense remains an active area of research (Chin et al., 2018; Farner & Lee, 2017; Lee et al., 2013; Tang et al., 2018; Turner & Langmuir, 2015; Turner et al., 2016), thick crust and crystal fractionation are not necessary for the generation of oxidized magmas.

***Inferences about Mantle fO_2* as a Function of Tectonic Setting.** From the analysis above, we may conclude that neither degassing nor crystal fractionation can generate the increases we observe in $Fe^{3+}/\Sigma Fe$ ratios as we move from the mid-ocean ridge, to the back-arc, to the arc-front environment. The inability of these processes to greatly alter fO_2 is evidenced by the fact that magnetite–ilmenite oxybarometry on volcanics, and spinel-oxybarometry on the source mantle itself, also record increasing fO_2 as we

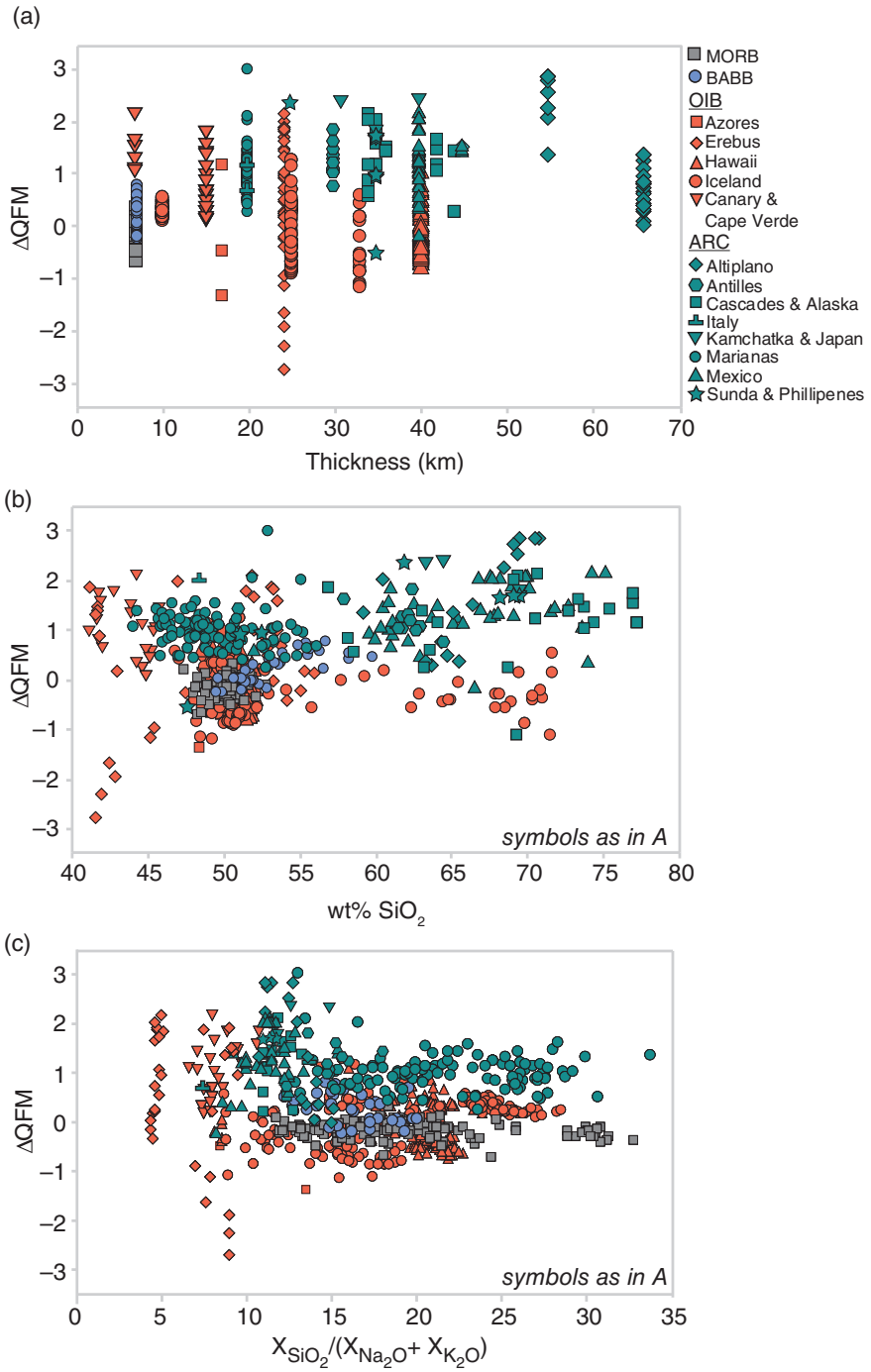

Figure 3.6 Magmatic oxygen fugacity as recorded by volcanics for samples in our compilation as a function of the crustal thickness (a) and SiO_2 (b), and the molar ratio of SiO_2/Na_2O+K_2O (c). We combine oxygen fugacities derived from melt inclusions with those from magnetite-ilmenite pairs for each tectonic setting in each panel; we do not distinguish results based on method. Crustal thickness taken from (Behn & Grove, 2015; Calvert et al., 2008; Chulick et al., 2013; Darbyshire et al., 2000; Das & Nolet, 1998; Ferrari et al., 2012; Finotello et al., 2011; Janiszewski et al., 2013; Levin et al., 2002; Manalo et al., 2015; McGlashan et al., 2008; Nicolich et al., 2000; Saiga et al., 2010; Sevilla et al., 2010; Spieker et al., 2018; Syuhada et al., 2016; Takahashi et al., 2007; Veenstra et al., 2006; Watts & ten Brink, 1989).

move from the ridge, to the back-arc, to the subduction-influenced forearc, to the arc-front setting. We conclude from this evidence that the mantle source itself must become oxidized as the influence of subduction increases. Indeed, *in situ* work by Kelley and Cottrell (2009) and numerous studies since (Brounce et al., 2014; Brounce et al., 2021; Brounce et al., 2015; Kelley & Cottrell, 2012), have linked the fO_2 recorded by submarine glasses and olivine-hosted melt inclusions to enrichment in slab-derived fluid-mobile incompatible trace elements. However, it is critical to consider other lines of evidence, such as trace element proxies, that have been argued to be more robust proxies for mantle fO_2 (e.g., Lee et al., 2005).

We compare our Fe-based oxybarometry results to those obtained from trace element partitioning. Several studies based on V/Sc, V/Y, V/Ti, V/Ga, Zn/Fe ratios, or Cu concentrations have concluded that the fO_2 recorded by arc volcanics are statistically indistinguishable from those recorded by MORB (Lee et al., 2005; Lee et al., 2010; Lee et al., 2012; Mallmann & O'Neill, 2013); this study, and others, have reached the opposite conclusion (Bucholz & Kelemen, 2019; Laubier et al., 2014; Shervais, 1982). It is beyond the scope of this contribution to translate the V/Yb ratios we have compiled into fO_2; however, the conclusion that V/Yb of MORB < BABB < arc basalts is robust (Figure 3.4). This implies that subduction-modified mantle is more oxidized than the MORB source mantle, consistent with Fe-based oxybarometry, for reasons that remain debated (e.g., Andreani et al., 2013; Benard et al., 2018; Canil & Fellows, 2017; Carmichael, 1991; Chin et al., 2018; Debret et al., 2014; Evans, this volume; Farner & Lee, 2017; Foden et al., 2018; Gaillard et al., 2015; Kelley & Cottrell, 2009; Lecuyer & Ricard, 1999; Lee et al., 2005; Mungall, 2002; Nebel et al., 2015; Parkinson & Arculus, 1999; Tang et al., 2018; Tollan & Hermann, 2019; Williams et al., 2004; Wood et al., 1990).

3.5. CONCLUSIONS AND FUTURE DIRECTIONS

Oxygen fugacity varies as a function of tectonic setting. We have shown that all estimators of magmatic fO_2 (XANES, magnetite-ilmentite pairs) and mantle source fO_2 (spinel oxybarometry, V/Yb ratio) show independently that the fO_2 of ridges < back-arcs < arcs. Inferences about plume fO_2 are strongly model dependent, and our study indicates that plume fO_2s range widely, but on average are similar to or higher than mid-ocean ridges. We also strongly conclude that mantle lithologies record a much greater range in fO_2 than volcanics.

The process of subduction generates elevated fO_2 in both melts and mantle lithologies, though the mechanism and locus of this shift remains debated. The extent to which arc rocks are oxidized relative to MORB does not correlate with crustal thickness or indices of crystal fractionation. Degassing may oxidize or reduce magmas to small extents (< 0.2 log units) so long as melts are captured at pressures > 500 bar, and the tendency for shallow degassing (< 200 bar) to reduce magmas appears universal across all tectonic settings. Plate recycling may also enable plumes to achieve their elevated fO_2 relative to mid-ocean ridges; however, when attempting to project back to near-primary compositions, the fO_2 of plume lithologies is uncertain. This is because plume volcanics have thus far only constrained fO_2 minima, and because plume xenoliths derive from lithospheric mantle that was generated at distal mid-ocean ridges that have subsequently metamorphosed and are variably overprinted by the passage of transiting plume-derived melts.

Several additional challenges confront a more complete understanding of oxygen fugacity as a function of tectonic setting. Geographic coverage of fO_2 estimates remains poor, with peridotites from ridges, volcanic rocks and xenoliths from plumes, and primitive volcanic rocks from arcs especially so. Further sampling of primitive melts and mantle lithologies from diverse tectonic environments is needed in order to illuminate the geodynamic and compositional origins of variable fO_2 across tectonic settings. Analytical challenges must still be overcome. Some of the most promising samples for the elucidation of redox processes – melt inclusions – are difficult to prepare and susceptible to radiation beam damage (Cottrell et al., 2018). Experiments and models are needed to gain insights into processes that may shift the fO_2s recorded by melts and residues during partial melting of the source and after melt and residue separate. Additional observations of natural samples and new experiments and models are required to ultimately connect the fO_2 recorded by partial melts, peridotites and pyroxenites, and the fO_2 of the solid convecting mantle.

ACKNOWLEDGMENTS

We thank Oliver Shorttle for providing his XANES data reprocessed using the updated calibration of Zhang et al. (2018). We are grateful to Paolo Sossi, Frank Spera, and an anonymous reviewer for thoughtful, detailed, and constructive comments that greatly improved this contribution. We thank Roberto Moretti and Daniel Neuville for organizing the monograph and for extending the invitation to submit. EC thanks the Lyda Hill Foundation for support during preparation of this manuscript.

METHODS APPENDIX

OXYGEN FUGACITY CALCULATIONS

Volcanics

a. Magnetite-Ilmenite Pairs

For arc and ocean island volcanics, we collected previously reported compositions of magnetite and ilmenite from 28 studies (Arce et al., 2013; Baggerman & DeBari, 2011; Beier et al., 2006; Browne et al., 2010; Carmichael, 1967, 1964; Coombs & Gardner, 2001; Costa et al., 2004; Crabtree & Lange, 2011; Crabtree & Waters, 2017; Devine et al., 2003; Ferrari et al., 2012; Frey and Lange, 2011; Genske et al., 2012; Grocke et al., 2017; Grove et al., 2005; Gunnarsson et al., 1998; Howe et al., 2014; Izbekov et al., 2002; Larsen, 2006; Muir et al., 2014; Portnyagin et al., 2012; Stelten & Cooper, 2012; Toothill et al., 2007; Wallace & Carmichael, 1994; Waters et al., 2015; Wolfe et al., 1997; Wright, 1972). We applied the equilibrium criteria of Bacon & Hirschman (1988) to all collected oxide compositions and only use those that pass for calculations of temperature and oxygen fugacity. (Equilibrium between ilmenite and magnetite is assessed based on comparison Mn and Mg partitioning between ilmenite and magnetite pairs with a dataset of magnetite-ilmenite pairs from natural volcanics inferred to be at equilibrium), Oxide compositions were input into the model of Ghiorso and Evans (2008) to obtain temperatures and oxygen fugacities. Ghiorso and Evans (2008) report their error for the parameterization of their model in terms of the residual energies (kJ) associated with the exchange and redox equilibria between magnetite and ilmenite. We evaluate the uncertainty of the model of Ghiorso & Evans (2008) by comparing modeled values of temperature and oxygen fugacity for experimentally grown iron oxide pairs with the reported experimental conditions (see Fig. 10 from Ghiorso & Evans, 2008). We find the uncertainty in oxygen fugacity and temperatures associated with model of Ghiorso and Evans (2008) is ±0.25 log units and ±45°C, respectively. All temperatures and oxygen fugacities obtained from magnetite-ilmenite pairs are shown in Figure A1.

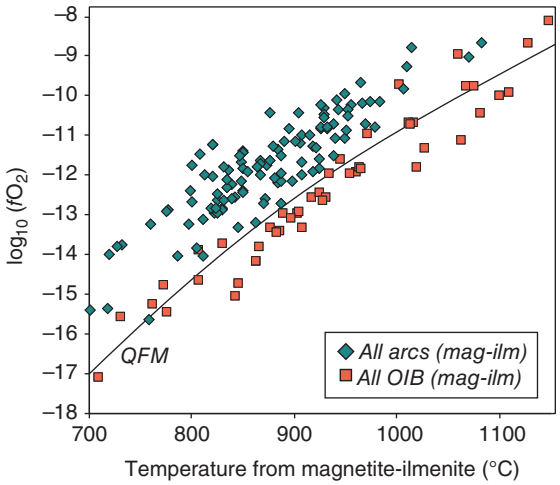

Figure A1 Temperatures and values of fO_2 from the model of Ghiorso and Evans (2008) and all magnetite–ilmenite pairs and used in this study.

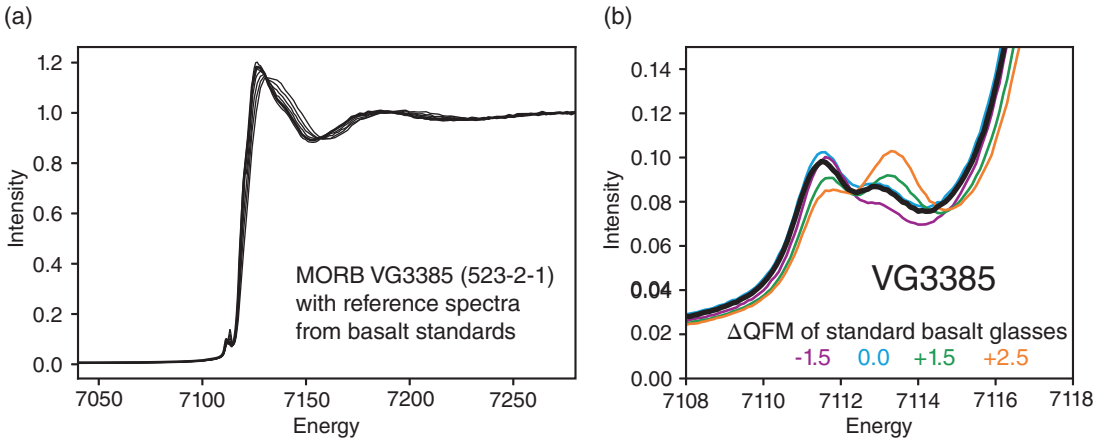

Figure A2 XANES spectra of MORB glass VG3385 with spectra of mid-ocean ridge basalt equilibrated over a range of fO_2, modified from Fig. 1 of Cottrell and Kelley (2011). The spectra of published MORB glasses fall between basalts equilibrated at furnace fO_2s of QFM-0.71 to QFM +0.87. XANES spectroscopy strongly indicates a narrow distribution of MORB fO_2 around QFM, regardless of the corresponding $Fe^{3+}/\Sigma Fe$ of the glasses.

b. ***$Fe^{3+}/\Sigma Fe$ ratios from XANES***

We calculate magmatic fO_2s from measured $Fe^{3+}/\sum Fe$ ratios using Kress and Carmichael (1991) and referenced to the QFM oxygen buffer of Frost (1991) at one atmosphere and 1200 °C, using the major element compositions reported by each study. For studies that quantify $Fe^{3+}/\sum Fe$ ratios using the standard glasses of Cottrell et al. (2009; see Table 3.1), we have recalculated those $Fe^{3+}/\sum Fe$ ratios according to a revision of the Mössbauer-determined $Fe^{3+}/\sum Fe$ ratios of those standard glasses (Zhang et al., 2018). Oliver Shorttle (pers. comm.) provided us with his revised $Fe^{3+}/\sum Fe$ ratios based on the Zhang et al. (2018) update.

c. ***Application of Kress and Carmichael (1991)***

A subset of the data we compiled for this review reports glass $Fe^{3+}/\Sigma Fe$ ratios. Unlike mineral equilibria, we must relate glass $Fe^{3+}/\Sigma Fe$ ratios to fO_2 via an empirical model

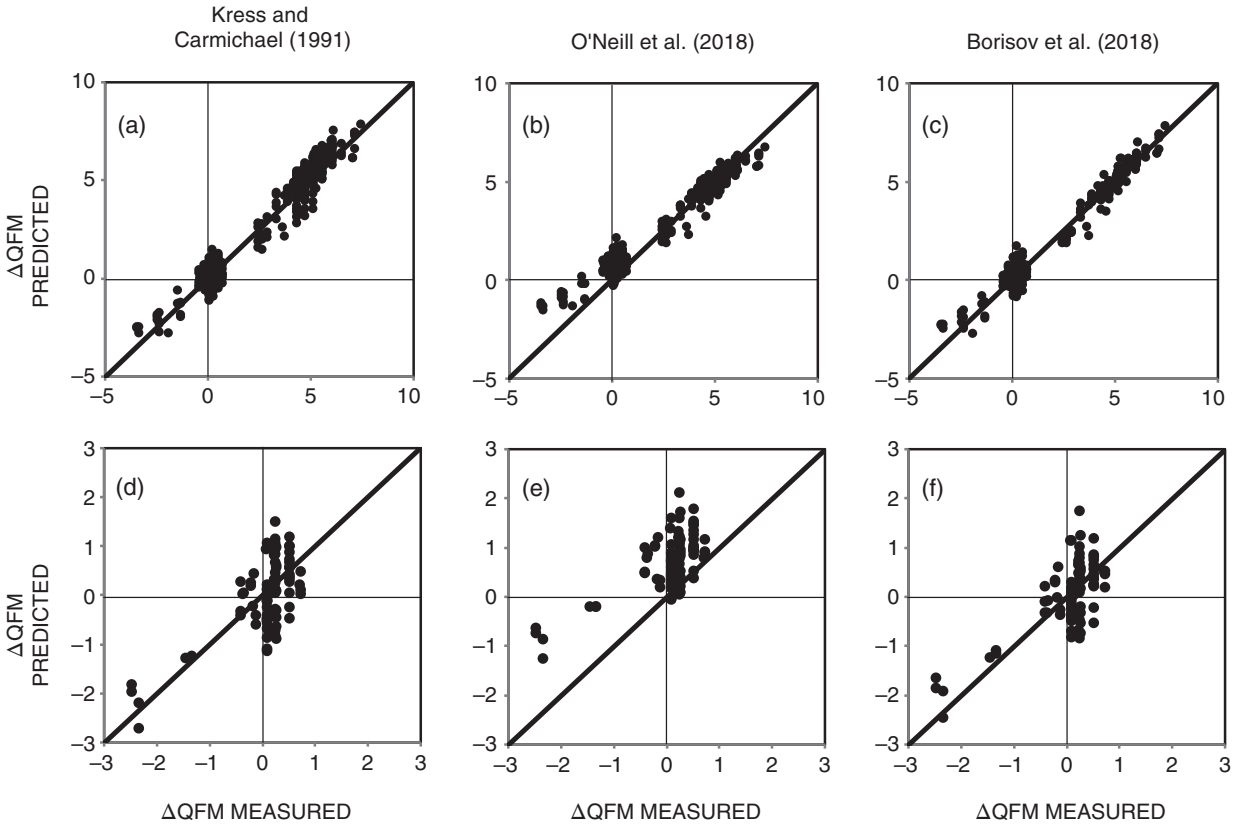

Figure A3 The measured experimental furnace fO_2 in log units relative to the QFM buffer for Borisov et al. (2018)'s recent compilation of 435 controlled-atmosphere experiments vs the fO_2 predicted by three fO_2 parameterizations (i.e. calculated fO_2 from the inputs of $Fe^{3+}/\Sigma Fe$ ratio, T, and major element composition). (a–c) Furnace fO_2 predicted by each parameterization for 435 compositions from QFM -3.3 to +7.3, and (d–f) for 98 "terrestrial" compositions (see Table A1) in the Earth-relevant fO_2 range of QFM -3 to +3. Panels (a) and (d) use the parameterization of Kress and Carmichael (1991); panels (b) and (e) use the parameterization of O'Neill et al. (2018); panels (c) and (f) use the parameterization of Borisov et al. (2018).

Table A1 Major element criteria for "terrestrial" lavas between QFM -3 and QFM +4.1 and "MORB-like" lavas between QFM -2 and QFM +2

	SiO_2	TiO_2	FeO	Na_2O	Al_2O_3	CaO	MgO	K_2O	MnO	P_2O_5
"terrestrial" N=98	42–78	0–4	0.1–18	1–6	11–23	0.1–15	1–14	0–6	0–0.5	0–2
MORB-like N=33	45–55	0.5–4	6–16	1.5–4	12–18	8–14	4–12	0–3	0–0.4	0–1

Major element ranges equal or exceed (Basaltic Volcanism Study Project, 1981) and (Ewart, 1979)

that accounts for composition. Several studies parameterize the relationship between $Fe^{3+}/\Sigma Fe$ ratio and fO_2 and a detailed comparison can be found in Borisov et al. (2018). For this compilation, we investigated those of Borisov et al. (2018), O'Neill et al. (2018), and Kress and Carmichael (1991). [During preparation of this manuscript, a typo in O'Neill et al. (2018) came to light; the coefficient for P_2O_5 in Eqn. 9b in the text of O'Neill et al. (2018) should be –0.018 not –0.18 as written. We use the correct equation here.]

The Borisov et al. (2018) and Kress and Carmichael (1991) models are both empirical parameterizations of hundreds of wet-chemical determinations of $Fe^{3+}/\Sigma Fe$ ratios of glasses of diverse compositions equilibrated in controlled-atmosphere experiments. O'Neill et al. (2018) heavily weights ("anchors") their calibration with the Mössbauer determinations of $Fe^{3+}/\Sigma Fe$ ratios of basalts (one basalt composition from Berry et al. (2018), two basalt compositions from Cottrell et al. (2009), but with the $Fe^{3+}/\Sigma Fe$ ratios "corrected" to be consistent with Berry et al. (2018), one low-Fe basalt composition from Jayasuriya et al. (2004), and one high-Fe sherggotite from Righter et al. (2013), but without that study's correction for recoilless fraction). They then derive the compositional terms from approximately the same database of wet-chemical results used in the Borisov et al. (2018) and Kress and Carmichael (1991) models, though O'Neill et al. (2018) uses only compositions with < 60 wt.% SiO2. Not included was the Mössbauer study of Zhang et al. (2018), which determined recoilless fraction using cryogenic Mössbauer. Correction for recoilless fraction reduces the $Fe^{3+}/\Sigma Fe$ ratios of Cottrell et al. (2009) by a few percent absolute, though this decrease is not equivalent to the "correction" applied by O'Neill et al. (2018). The Mössbauer studies of Zhang et al. (2018) and Berry et al. (2018) obtain fundamentally different results. We prefer the Mössbauer treatment of Zhang et al. (2018) because the methods applied in Berry et al. (2018) depend on assumptions we believe are flawed, including that highly reduced basalt is free of ferric iron (even under the most reducing conditions, Fe^0 coexists with substantial Fe^{3+} (Allen & Snow, 1955; Bowen & Schairer, 1932); that hyperfine parameters remain constant as $Fe^{3+}/\Sigma Fe$ ratio varies (there is ample evidence to the contrary, e.g., Mysen, 2006); and that center shifts > 0.6, at low quadrupole splitting, should be assigned to ferrous iron (this assertion is unsupported, see Zhang et al., 2018 for a discussion). Of course, when exploring the accuracy of a technique, it is advantageous to cross-calibrate. We note that the calibration of Zhang et al. (2018) yields an fO_2- $Fe^{3+}/\Sigma Fe$ ratio relationship that is the same within uncertainty as Kress and Carmichael (1991) model and Borisov et al. (2018) model, based on independent wet-chemical measurements (see also Partzsch et al., 2004), and spinel oxybarometry (Davis & Cottrell, 2018). Debate on these points must play out in the peer-reviewed literature and so for the purpose of this compilation, we take a different, agnostic, approach.

For our assessment, we take advantage of the fact that electrochemical sensors, the devices that monitor the fO_2 within gas-mixing furnaces, are accurate to better than ±0.1 log units in fO_2 and yield oxybarometric results consistent with independent calorimetric data, even accounting for potential interlaboratory biases due to poor calibration of the furnace hotspot (O'Neill & Pownceby, 1993). Taking advantage of this precision and accuracy, we use Borisov et al. (2018)'s recent compilation of 435 controlled-atmosphere experiments to assess the parameterizations; the same experimental database that provides the compositional terms in all three parameterizations. The 435 experiments have wet-chemical determinations of $Fe^{3+}/\Sigma Fe$ ratios, and so are independent of the aforementioned debate concerning Mössbauer spectroscopy. We calculated the furnace fO_2 predicted by each parameterization for 435 compositions from QFM -3.3 to +7.3, and for 98 "terrestrial" compositions (Table A1) in the Earth-relevant fO_2 range of QFM -3 to +4.1.

Because our inputs are the experimental temperatures, reported major elements, and reported wet-chemical determinations of $Fe^{3+}/\Sigma Fe$ ratios of the experiments, this analysis makes no assumptions about the accuracy of the data that underlie O'Neill et al. (2018), Borisov et al. (2018), or Kress and Carmichael (1991). This analysis only asks how well the three parameterizations predict the known furnace fO_2 of those 435 experiments given their independently-determined compositions. For the indicated terrestrial range, O'Neill et al. (2018)'s parameterization returns furnace fO_2s that are, on average, 0.56 (±0.55) log units higher than measured, Kress and Carmichael (1991)'s returns furnace fO_2s that are 0.09 (±0.58) lower than measured, and Borisov et al., (2018)'s returns 0.05 (±0.52) lower than measured. Standard errors on the estimates are reported in Table A2. We could therefore move forward confidently with either Kress and Carmichael (1991) or Borisov et al. (2018) but use the former simply because we had completed our analysis before Borisov et al. (2018) was published. Table A2 reports the standard error of each parameterization for the entire compilation and compositional subsets as defined in Table A1. Our analysis assumes that there is no systematic inaccuracy amongst the wet-chemical studies compiled by Borisov et al., (2018). O'Neill et al. (2018) raise the possibility that some wet-chemical determinations could be erroneous, and cite four suspect studies. Of these four, only two are included in the compilation of Borisov et al. (2018), and of these, 80% are from the study of Thornber et al. (1980). We therefore assessed whether

Table A2 Standard error (σ_{est}) of three fO_2 parameterizations.

	n=435	n=98	n=33
reference	(all expts compiled by [Borisov et al., 2018])	("terrestrial" lavas)	("MORB-like" lavas)
Kress & Carmichael, 1991	0.56	0.59	0.53
Hugh St C. O'Neill et al., 2018	0.58	0.79	0.8
Borisov et al., 2018	0.38	0.53	0.49

inclusion/exclusion of the Thornber et al. (1980) data would significantly impact our analysis. It does not. For example, excluding data from Thornber et al. (1980) from the terrestrial data set (n = 55 without Thornber) causes the standard error of O'Neill et al. (2018) parameterization to degrade to 0.84, while the standard error of Kress and Carmichael (1991) stays constant and that of Borisov et al. (2018) improves to 0.50.

c. Vanadium oxybarometry using V/Yb ratios.

All method details provided in the main text.

Mantle Lithologies

We calculated the oxygen fugacity of mantle lithology (peridotites and olivine-orthopyroxene-spinel bearing pyroxenites) by spinel oxybarometry, following the procedures of Davis et al. (2017). This method uses phase equilibrium between olivine, orthopyroxene, and spinel to constrain the oxygen fugacity of the system.

Calculated oxygen fugacity values are highly dependent on mineral activity models. We have thus recalculated all literature data to use a single set of activity models. For olivine and orthopyroxene, we use the activity models cited in Wood and Virgo (1989). For spinel, we use the activity model developed by Sack and Ghiorso (1991a, b). This spinel activity model better reproduces the experimental data of Wood (1990) than do other commonly used spinel activity models such as those of Mattioli and Wood (1988) and Nell and Wood (1991) (see Davis et al., 2017, for further discussion). Additionally, the Sack and Ghiorso (1991a,b) model is more applicable to spinels at high Cr#, such as the arc and forearc peridotites reported in this work (see Birner et al., 2017, for further discussion).

The activity of magnetite in spinel is itself highly dependent on accurate determination of the ferric iron content within the spinel phase. The studies included in this compilation determine ferric iron content in spinel using either Mössbauer spectroscopy or electron probe microanalysis (EPMA). In the case of EPMA, ferric iron content cannot be determined directly and is instead calculated using stoichiometric constraints. The preferred method of determining ferric iron content in this manner involves correcting the values based on a set of calibration spinels, with ferric iron contents independently determined by Mössbauer, run at the beginning and end of each EPMA session (e.g., Wood & Virgo, 1989; Davis et al., 2017). For peridotites from ridges, arcs, and forearcs compiled in this study, we have only included data in which the $Fe^{3+}/\sum Fe$ ratio of spinel was determined via Mössbauer or corrected EPMA. In the case of xenoliths from OIB localities, we have chosen to additionally include a number of studies in which this correction was not applied, due to the paucity of measurements using spinel standards for correction. Uncertainty in fO_2 increases when uncorrected EPMA analyses of spinels are used to calculate fO_2, but the degree to which that uncertainty increases is dependent on the $Fe^{3+}/\sum Fe$ ratio of the spinel. Uncertainty in fO_2 is greater for spinels with lower $Fe^{3+}/\sum Fe$ ratios and lesser for spinels with higher $Fe^{3+}/\sum Fe$ ratios (Ballhaus et al. 1991; Davis et al. 2017). For example, fO_2 calculated from corrected EPMA analyses of spinels with $Fe^{3+}/\sum Fe = 0.10$ has an fO_2 uncertainty of about +0.3/-0.4 log units, whereas the uncertainty roughly doubles for uncorrected spinel analyses. At $Fe^{3+}/\sum Fe > 0.35$, fO_2 uncertainty is only about 0.1 log units for corrected EPMA analyses, and doubles to about 0.2 log units when the analyses are uncorrected. Therefore, the potential effects of including uncorrected analyses on the distribution of fO_2 recorded by peridotites from an oxidized setting is likely to be small.

The calculation of oxygen fugacity also depends highly on assumptions about the temperature and pressure of equilibration. In order to maintain consistency between datasets, we calculate the fO_2 values of all mantle lithologies at 0.6 GPa and the temperature recorded by spinel-olivine thermometry. Justification for this choice can be found in Birner et al. (2017) for forearc/arc peridotites and Birner et al. (2018) for mid-ocean ridge peridotites. Although we choose these values to maintain consistency, there is no rigorous method available to estimate pressure recorded by spinel peridotite xenoliths and no thermal model that can be easily applied to plume-influenced lithosphere that would allow recorded temperature to be related to a depth along a geotherm. OIB xenoliths could potentially have been exhumed from any depth within the spinel stability field. Assuming a maximum pressure of 2.5 GPa, the choice to calculate fO_2 at 0.6 GPa may lead to an overestimation of fO_2 relative to QFM by as much as 0.6 to 0.8 log units. This difference

in fO_2 relative to QFM is owing to the differences in ΔV of the QFM reaction and the reaction underlying the spinel oxybarometer (fayalite-ferrosilite-magnetite).

Modeling in DCompress. We modeled the change in magmatic fO_2 with progressive degassing of a C-O-H-S vapor using the gas-melt equilibrium model of Burgisser et al. (2015). This thermodynamic model computes C, H, O, and S concentrations and speciation in coexisting gas and silicate melt as functions of pressure, temperature, melt composition, and fO_2, based on experimental calibrations of melt solubility and homogeneous equilibrium in the gas phase for H2, H2O, CO, CO_2, SO_2, H2S, and S2 species. The melt does not change in major element composition during degassing (i.e., there is no crystallization) and it is not permitted to precipitate separate sulfide or carbon phases.

We followed the methodology of Brounce et al. (2017) to compute the degassing trajectories, except that we used the DCompress default solubility models for C-O-H-S species. We used the default basalt composition and non-temperature dependent solubility relationships of H2, H2O, CO_2, H2S, and SO_2. We also executed model runs wherein we set the solubility of H2 in the silicate melt to zero in order to demonstrate how uncertainty in the speciation of H-species in silicate melts (e.g., finite solubility [Hirschmann et al., 2012; Mysen et al., 2011] vs no solubility ([Newcombe et al., 2017]) propagates into uncertainty in degassing trajectories, particularly those at relatively low fO_2. Among these simulations, only the scenario of an arc magma decompressing at QFM= 0 (i.e., H2O-rich magma in equilibrium with a gas phase containing non-negligible amounts of H2) was sensitive to this assumption (Fig. 3.5). All calculations are calculated as equilibrium (i.e., batch) isothermal decompression, at 1100 °C. The calculations intended to simulate MORB degassing were started at QFM and 1385 bar, with concentrations of volatiles similar to those calculated for globally representative primary MORB melts (Le Voyer et al., 2018) containing 0.2 wt.% H2O, 1100 ppm C_{O2}, and 1425 ppm S. Increasing CO_2 to several thousand ppm has no effect on the trajectories shown. The calculations intended to simulate OIB degassing were started at QFM +1.4 and 2115 bar, with concentrations of volatiles similar to those expected for undegassed Erebus melts (Mousallam et al., 2014) containing 1.5 wt% H_2O, 1710 ppm CO_2, and 2430 ppm S. The calculations intended to simulate arc degassing were started at QFM +1.5 and 2380 bar, with concentrations of volatiles similar to those observed in melt inclusions from Agrigan volcano, containing 4.5 wt.% H_2O, 800 ppm CO_2, and 2050 ppm S (e.g., Kelley & Cottrell, 2012). Melt chemistry (including fO_2) and gas phase compositions were calculated in 1 bar increments and stopped at 5 bars (total pressure).

REFERENCES

Allen, W., & Snow, R. (1955). The orthosilicate-iron oxide portion of the system CaO-"FeO"-SiO2. *Journal of the American Ceramic Society*, *38*(8), 264–272.

Anderson, A. T., & Wright, T. L. (1972). Phenocrysts and glass inclusions and their bearing on oxidation and mixing of basaltic magmas, Kilauea Volcano, Hawaii. *American Mineralogist*, *57*(1–2), 188–216.

Andreani, M., Munoz, M., Marcaillou, C., & Delacour, A. (2013). u-XANES study of iron redox state in serpentine during oceanic serpentinization. *Lithos*, *178*, 70–83. doi: 10.1016/j.lithos.2013.04.008

Arce, J. L., Gardner, J. E., & Macias, J. L. (2013). Pre-eruptive conditions of dacitic magma erupted during the 21.7 ka Plinian event at Nevado de Toluca volcano, Central Mexico. *Journal of Volcanology and Geothermic Research*, *249*, 49–65. doi: 10.1016/j.jvolgeores.2012.09.012

Bacon, C. R., & Hirschmann, M. M. (1988). Mg/Mn Partitioning as a Test for Equilibrium between Coexisting Fe-Ti Oxides. *American Mineralogist*, *73*(1–2), 57–61.

Baggerman, T. D., & DeBari, S. M. (2011). The generation of a diverse suite of Late Pleistocene and Holocene basalt through dacite lavas from the northern Cascade arc at Mount Baker, Washington. *Contributions to Mineralogy and Petrology*, *161*(1), 75–99. doi: 10.1007/s00410-010-0522-2

Bali, E., Keppler, H., & Audetat, A. (2012). The mobility of W and Mo in subduction zone fluids and the Mo–W–Th–U systematics of island arc magmas. *Earth and Planetary Science Letters*, *351–352*, 195–207. doi: 10.1016/j.epsl.2012.07.032

Ballhaus, C. (1993). Redox States of Lithospheric and Asthenospheric Upper-Mantle, *Contributions to Mineralogy and Petrology*, *114*(3), 331–348.

Ballhaus, C., Berry, R. F., & Green, D. H. (1991). High-pressure experimental calibration of the olivine-ortho-pyroxene-spinel oxygen geobarometer - implications for the oxidation-state of the upper mantle. *Contributions to Mineralogy and Petrology*, *107*(1), 27–40.

Basaltic Volcanism Study Project. (1981). *Basaltic volcanism of the terrestrial planets*, New York: Pergamon Press Inc. 1286 pp.

Behn, M. D., & Grove, T. L. (2015). Melting systematics in mid-ocean ridge basalts: Application of a plagioclase-spinel melting model to global variations in major element chemistry and crustal thickness. *Journal of Geophysical Research: Solid Earth*, *120*(7), 4863–4886.

Beier, C., Haase, K. M., & Hansteen, T. H. (2006). Magma evolution of the Sete Cidades volcano, Sao Miguel, Azores. *Journal of Petrology*, *47*(7), 1375–1411. doi: 10.1093/petrology/egl014

Benard, A., Klimm, K., Woodland, A. B., Arculus, R. J., Wilke, M., Botcharnikov, R. E., et al. (2018). Oxidising agents in sub-arc mantle melts link slab devolatilisation and arc magmas. *Nature Communications*, *9*. doi: 10.1038/s41467-018-05804-2.

Bénard, A., Woodland, A. B., Arculus, R. J., Nebel, O., & McAlpine, S. R. B. (2018). Variation in sub-arc mantle oxygen fugacity during partial melting recorded in refractory

peridotite xenoliths from the West Bismarck Arc. *Chemical Geology*, *486*, 16–30. doi: 10.1016/j.chemgeo.2018.03.004

Berry, A. J., Stewart, G. A., O'Neill, H. S. C., Mallmann, G., & Mosselmans, J. F. W. (2018). A re-assessment of the oxidation state of iron in MORB glasses. *Earth and Planetary Science Letters*, *483*, 114–123. doi: https://doi.org/10.1016/j.epsl.2017.11.032

Bezos, A., Guivel, G., La, C., Fougeroux, T., & Humler, E. (2021). Unraveling the confusion over the iron oxidation state in MORB glasses. *Geochimica et Cosmochimica Acta*, *293*, 28–39. doi: https://doi.org/10.1016/j.gca.2020.10.004

Bezos, A., & Humler, E. (2005). The Fe3+/Sigma Fe ratios of MORB glasses and their implications for mantle melting. *Geochimica et Cosmochimica Acta*, *69*(3), 711–725.

Birner, S. K., Cottrell, E., Warren, J. M., Kelley, K. A., & Davis, F. A. (2018). Peridotites and basalts reveal broad congruence between two independent records of mantle fO_2 despite local redox heterogeneity. *Earth and Planetary Science Letters*, *494*, 172–189.

Birner, S. K., Warren, J. M., Cottrell, E., Davis, F. A., Kelley, K. A., & Falloon, T. J. (2017). Forearc peridotites from Tonga record heterogeneous oxidation of the mantle following subduction initiation. *Journal of Petrology*, *58*(9), 1755–1780.

Bonadiman, C., Beccaluva, L., Coltorti, M., & Siena, F. (2005). Kimberlite-like metasomatism and 'garnet signature'in spinel-peridotite xenoliths from Sal, Cape Verde Archipelago: relics of a subcontinental mantle domain within the Atlantic oceanic lithosphere? *Journal of Petrology*, *46*(12), 2465–2493.

Bonnin-Mosbah, M., Simionovici, A. S., Metrich, N., Duraud, J. P., Massare, D., & Dillmann, P. (2001). Iron oxidation states in silicate glass fragments and glass inclusions with a XANES micro-probe. *Journal of Non-Crystalline Solids*, *288*(1–3), 103–113.

Borisov, A., Behrens, H., & Holtz, F. (2018). Ferric/ferrous ratio in silicate melts: a new model for 1 atm data with special emphasis on the effects of melt composition. *Contributions to Mineralogy and Petrology*, *173*(12), doi: 10.1007/s00410-018-1524-8

Bowen, N. L., & Schairer, J. F. (1932). The System, FeO-SiO2, *American Journal of Science*, *24*(141), 177–213.

Brandon, A. D., & Draper, D. S. (1996). Constraints on the origin of the oxidation state of mantle overlying subduction zones: An example from Simcoe, Washington, USA. *Geochimica et Cosmochimica Acta*, *60*(10), 1739–1749.

Brounce, M., Kelley, K., & Cottrell, E. (2014). Variations in Fe3+/$\sum$ Fe of Mariana arc basalts and mantle wedge fO_2. *Journal of Petrology*, *55*(12), 2513–2536.

Brounce, M., Reagan, M., Kelley, K. A., Cottrell, E., Shimizu, K., & Almeev, R. (2021). Co-variation of slab tracers, volatiles, and oxidation during subduction initiation. *Geochemistry, Geophysics, Geosystems*. doi: https://doi.org/10.1029/2021GC009823

Brounce, M., Stolper, E., & Eiler, J. (2017). Redox variations in Mauna Kea lavas, the oxygen fugacity of the Hawaiian plume, and the role of volcanic gases in Earth's oxygenation. *Proceedings of the National Academy of Sciences of the United States of America*, *114*(34), 8997–9002. doi: https://10.1073/pnas.1619527114

Brounce, M., Cottrell, E., & Kelley, K. A. (2019). The redox budget of the Mariana subduction zone. *Earth and Planetary Science Letters*, *528*. doi: Doi.org/10.1016/j.epsl.2019.115859

Brounce, M., Kelley, K. A., Cottrell, E., & Reagan, M. K. (2015). Temporal evolution of mantle wedge oxygen fugacity during subduction initiation. *Geology*, *43*(9), 775–778. doi: 10.1130/G36742.1

Browne, B., Izbekov, P., Eichelberger, J., & Churikova, T. (2010). Pre-eruptive storage conditions of the Holocene dacite erupted from Kizimen Volcano, Kamchatka. *International Geology Review*, *52*(1), 95–110. doi: 10.1080/00206810903332413

Bryndzia, L. T., & Wood, B. J. (1990). Oxygen thermobarometry of abyssal spinel peridotites - The redox state and C-O-H volatile composition of the Earth's sub-oceanic upper mantle. *American Journal of Science*, *290*(10), 1093–1116.

Bucholz, C. E., & Kelemen, P. B. (2019). Oxygen fugacity at the base of the Talkeetna arc, Alaska. *Contributions to Mineralogy and Petrology*, *174*(10). doi: 10.1007/s00410-019-1609-z

Buddington, A., & Lindsley, D. (1964). Iron-titanium oxide minerals and synthetic equivalents. *Journal of Petrology*, *5*(2), 310–357.

Burgisser, A., Alletti, M., & Scaillet, B. (2015). Simulating the behavior of volatiles belonging to the C–O–H–S system in silicate melts under magmatic conditions with the software D-Compress. *Computers & Geosciences*, *79*, 1–14. doi: 10.1016/j.cageo.2015.03.002

Calvert, A. J., Klempere, S. L., Takahashi, N., & Kerr, B. C. (2008). Three-dimensional crustal structure of the Mariana island arc from seismic tomography. *Journal of Geophysical Research*, *113*, B01406.

Canil, D. (1990). Experimental study bearing on the absence of carbonate in mantle-derived xenoliths. *Geology*, *18*, 1011–1013.

Canil, D. (1997). Vanadium partitioning and the oxidation state of Archaean komatiite magmas. *Nature*, *389*(6653), 842–845.

Canil, D. (2002). Vanadium in peridotites, mantle redox and tectonic environments: Archean to present. *Earth and Planetary Science Letters*, *195*(1–2), 75–90.

Canil, D., & Fellows, S. A. (2017). Sulphide–sulphate stability and melting in subducted sediment and its role in arc mantle redox and chalcophile cycling in space and time. *Earth and Planetary Science Letters*, *470*, 73–86. doi: 10.1016/j.epsl.2017.04.028

Carmichael, I. S. E. (1967). The mineralogy of thingmuli, a tertiary volcano in Eastern Iceland. *American Mineralogist*, *52*, 1815–1841.

Carmichael, I. S. E. (1991). The redox states of basic and silicic magmas - a reflection of their source regions. *Contributions to Mineralogy and Petrology*, *106*(2), 129–141.

Carmichael, I. S. E., & Nicholls, J. (1967). Iron-titanium oxides and oxygen fugacities in volcanic rocks. *Journal of Geophysical Research*, *72*(18), 4665–4687.

Carmichael, I. S. E., & Ghiorso, M. S. (1986). Oxidation-reduction relations in basic magma - a case for homogeneous equilibria. *Earth and Planetary Science Letters*, *78*(2–3), 200–210.

Carroll, M. R., & Rutherford, M. J. (1988). Sulfur Speciation in Hydrous Experimental Glasses of Varying Oxidation-State - Results from Measured Wavelength Shifts of Sulfur X-Rays. *American Mineralogist*, *73*(7–8), 845–849.

Chin, E. J., Shimizu, K., Bybee, G. M., & Erdman, M. E. (2018). On the development of the calc-alkaline and tholeiitic magma series: A deep crustal cumulate perspective. *Earth and Planetary Science Letters*, *482*, 277–287. doi: 10.1016/j.epsl.2017.11.016

Christie, D. M., Carmichael, I. S. E., & Langmuir, C. H. (1986). Oxidation-states of Midocean Ridge basalt glasses. *Earth and Planetary Science Letters*, *79*(3–4), 397–411.

Chulick, G. S., Detweiler, S., & Mooney, W. D. (2013). Seismic structure of the crust and uppermost mantle of South America and surrounding oceanic basins. *Journal of South American Earth Sciences*, *42*, 260–276. doi: 10.1016/j.jsames.2012.06.002

Coombs, M. L., & Gardner, J. E. (2001). Shallow-storage conditions for the rhyolite of the 1912 eruption at Novarupta, Alaska. *Geology*, *29*(9), 775–778. doi: 10.1130/0091-7613(2001)029<0775:sscftr>2.0.co;2.

Cottrell, E., & Kelley, K. A. (2011). The oxidation state of Fe in MORB glasses and the oxygen fugacity of the upper mantle. *Earth and Planetary Science Letters*, *305*(3–4), 270–282. doi: 10.1016/j.epsl.2011.03.014

Cottrell, E., Kelley, K. A., Lanzirotti, A., & Fischer, R. A. (2009). High-precision determination of iron oxidation state in silicate glasses using XANES. *Chemical Geology*, *268*(3–4), 167–179. doi: 10.1016/j.chemgeo.2009.08.008

Cottrell, E., Birner, S. K., Brounce, M., Davis, F. A., Waters, L. E., & Kelley, K. A. (2021). Oxygen Fugacity Across Tectonic Settings, Version 1.0. Interdisciplinary Earth Data Alliance (IEDA). http://doi.org/10.26022/IEDA/111899

Cottrell, E., Lanzirotti, A., Mysen, B., Birner, S., Kelley, K. A., Botcharnikov, R., et al. (2018). A Mössbauer-based XANES calibration for hydrous basalt glasses reveals radiation-induced oxidation of Fe. *American Mineralogist: Journal of Earth and Planetary Materials*, *103*(4), 489–501.

Crabtree, S., & Lange, R. (2011). An evaluation of the effect of degassing on the oxidation state of hydrous andesite and dacite magmas: a comparison of pre- and post-eruptive Fe2 + concentrations. *Contributions to Mineralogy and Petrology*, *163*, 209–224. doi: 10.1007/s00410-011-0667-7

Crabtree, S. M., & Lange, R. A. (2011). Complex phenocryst textures and zoning patterns in andesites and dacites: Evidence of degassing-induced rapid crystallization? *Journal of Petrology*, *52*(1), 3–38. doi: 10.1093/petrology/egq067

Crabtree, S. M., & Waters, L. E. (2017). The petrologic history of the Sanganguey volcanic field, Nayarit, Mexico: Comparisons in a suite of crystal-rich and crystal-poor lavas. *Journal of Volcanology and Geothermic Research*, *336*, 51–67. doi: 10.1016/j.jvolgeores.2017.02.005.

Darbyshire, F. A., White, R. S., & Priestley, K. F. (2000). Structure of the crust and uppermost mantle of Iceland from a combined seismic and gravity study. *Earth and Planetary Science Letters*, *181*, 409–428.

Das, T., & Nolet, G. (1998). Crustal thickness map of the western United States by partitioned waveform inversion. *Journal of Geophysical Research: Solid Earth*, *103*(B12), 30021–30038.

Dasgupta, R., Jackson, M. G., & Lee, C.-T. A. (2010). Major element chemistry of ocean island basalts – Conditions of mantle melting and heterogeneity of mantle source. *Earth and Planetary Science Letters*, *289*(3–4), 377–392.

Dauphas, N., Craddock, P. R., Asimow, P. D., Bennett, V. C., Nutman, A. P., & Ohnenstetter, D. (2009). Iron isotopes may reveal the redox conditions of mantle melting from Archean to Present. *Earth and Planetary Science Letters*, *288*(1–2), 255–267.

Davis, F. A., & Cottrell, E. (2018). Experimental investigation of basalt and peridotite oxybarometers: implications for spinel thermodynamic models and Fe3+ compatibility during generation of upper mantle melts. *American Mineralogist*, *103*(7), 1056–1067. doi: http://doi.org/10.2138/am-2018-6280

Davis, F. A., Humayun, M., Hirschmann, M. M., & Cooper, R. S. (2013). Experimentally determined mineral/melt partitioning of first-row transition elements (FRTE) during partial melting of peridotite at 3GPa, *Geochimica et Cosmochimica Acta*, *104*, 232–260. doi: 10.1016/j.gca.2012.11.009

Davis, F. A., Cottrell, E., Birner, S. K., Warren, J. M., & Lopez, O. G. (2017). Revisiting the electron microprobe method of spinel-olivine-orthopyroxene oxybarometry applied to spinel peridotites. *American Mineralogist*, *102*(2), 421–435.

Debret, B., Andreani, M., Muñoz, M., Bolfan-Casanova, N., Carlut, J., Nicollet, C., et al. (2014). Evolution of Fe redox state in serpentine during subduction. *Earth and Planetary Science Letters*, *400*, 206–218. doi: 10.1016/j.epsl.2014.05.03

Devine, J. D., Rutherford, M. J., Norton, G. E., & Young, S. R. (2003). Magma storage region processes inferred from geochemistry of Fe-Ti oxides in andesitic magma, Soufriere Hills Volcano, Montserrat, WI. *Journal of Petrology*, *44*(8), 1375–1400. doi: 10.1093/petrology/44.8.1375

El-Rus, M. A. A., Neumann, E. R., & Peters, V. (2006). Serpentinization and dehydration in the upper mantle beneath Fuerteventura (eastern Canary Islands): Evidence from mantle xenoliths. *Lithos*, *89*(1), 24–46.

Elliott, T., Plank, T., Zindler, A., White, W., & Bourdon, B. (1997). Element transport from slab to volcanic front at the Mariana arc. *Journal of Geophysical Research: Solid Earth*, *102*(B7), 14991–15019.

Eugster, H. (1957). Heterogeneous reactions involving oxidation and reduction at high pressures and temperatures. *The Journal of Chemical Physics*, *26*(6), 1760–1761.

Eugster, H. P. (Ed.) (1959). *Oxidation and reduction in metamorphism*, New York: John Wiley & Sons. 397–426 pp.

Evans, K. A. (2021), Redox decoupling, redox budgets and magma recycling. In: D. R. Neuville and R. Moretti, (eds.) *AGU Geophysical Monograph Redox variables and mechanisms in magmatism and volcanism*. Wiley.

Evans, K. A., & Tomkins, A. G. (2011). The relationship between subduction zone redox budget and arc magma fertility. *Earth and Planetary Science Letters*, *308*, 401–409. doi: 10.1016/j.epsl.2011.06.009

Evans, K. A., Elburg, M. A., & Kamenetsky, V. S. (2012). Oxidation state of subarc mantle. *Geology*, *40*(9), 783–786. doi: 10.1130/g33037.1

Ewart, A. (1979). A review of the mineralogy and chemistry of Tertiary-recent dacitic, latitic, rhyolitic, and related salic volcanic rocks. *Developments in Petrology*, *6*, 13–121.

Farner, M. J., & Lee, C.-T. A. (2017). Effects of crustal thickness on magmatic differentiation in subduction zone volcanism: A global study. *Earth and Planetary Science Letters*, *470*, 96–107. doi: 10.1016/j.epsl.2017.04.025

Farnetani, C. G., & Hofmann, A. W. (2010). Dynamics and internal structure of the Hawaiian plume. *Earth and Planetary Science Letters*, *295*(1–2), 231–240. doi: 10.1016/j.epsl.2010.04.005

Ferrari, L., Orozco-Esquivel, T., Manea, V., & Manea, M. (2012). The dynamic history of the Trans-Mexican Volcanic Belt and the Mexico subduction zone. *Tectonophysics*, *522*, 122–149. doi: 10.1016/j.tecto.2011.09.018

Finotello, M., Nyblade, A., Julià, J., Wiens, D. A., & Anandakrishnana, S. (2011). Crustal Vp-Vs ratios and thicknesses for Ross Island and the Transantarctic Mountain front, Antarctica. *Geophysical Journal International*, *185*, 85–92.

Fleet, M. E., Liu, X., Harmer, S. L., & King, P. L. (2005). Sulfur K-edge XANES spectroscopy: Chemical state and content of sulfur in silicate glasses. *The Canadian Mineralogist*, *43*(5), 1605–1618.

Foden, J., Sossi, P. A., & Nebel, O. (2018). Controls on the iron isotopic composition of global arc magmas. *Earth and Planetary Science Letters*, *494*, 190–201. doi: 10.1016/j.epsl.2018.04.039

French, S. W., & Romanowicz, B. (2015). Broad plumes rooted at the base of the Earth's mantle beneath major hotspots. *Nature*, *525*, 95–99. doi: 10.1038/nature14876

Frey, F., & Roden, M. F. (1987). The mantle source for Hawaiian Islands. Constraints from the lavas and ultramafic inclusions. In: Menzies, M. A., & Hawkesworth, C. J. (Eds.) *Mantle Metasomatism*. London: Academic Press. pp. 423–463.

Frey, H. M., & Lange, R. A. (2011). Phenocryst complexity in andesites and dacites from the Tequila volcanic field, Mexico: resolving the effects of degassing vs. magma mixing. *Contributions to Mineralogy and Petrology*, *162*(2), 415–445. doi: 10.1007/s00410-010-0604-1

Frost, B. R. (Ed.) (1991). *Introduction to oxygen fugacity and its petrologic importance*, 1–9 pp. BookCrafters Inc., Chelsea, MI.

Frost, B. R., & Lindsley, D. H. (1992). Equilibria among Fe-Ti oxides, pyroxenes, olivine, and quartz 2. *Application American Mineralogist*, *77*(9–10), 1004–1020.

Frost, D. J., & McCammon, C. A. (2008). The redox state of Earth's mantle. *Annual Review of Earth and Planetary Sciences*, *36*(1), 389–420, doi: doi:10.1146/annurev.earth.36.031207.124322

Fryer, P., Ambos, E., & Hussong, D. (1985). Origin and emplacement of Mariana forearc seamounts. *Geology*, *13* (11), 774–777.

Gaetani, G. A., O'Leary, J. A., Shimizu, N., Bucholz, C. E., & Newville, M. (2012). Rapid reequilibration of H2O and oxygen fugacity in olivine-hosted melt inclusions. *Geology*, *40* (10), 915–918.

Gaillard, F., Scaillet, B., Pichavant, M., & Iacono-Marziano, G. (2015). The redox geodynamics linking basalts and their mantle sources through space and time. *Chemical Geology*, *418*, 217–233. doi: 10.1016/j.chemgeo.2015.07.030

Gale, A., Laubier, M., Escrig, S., & Langmuir, C. H. (2013a). Constraints on melting processes and plume-ridge interaction from comprehensive study of the FAMOUS and North Famous segments, Mid-Atlantic Ridge. *Earth and Planetary Science Letters*, *365*, 209–220. doi: 10.1016/j.epsl.2013.01.022

Gale, A., Dalton, C. A., Langmuir, C. H., Su, Y., & Schilling, J.-G. (2013b). The mean composition of ocean ridge basalts. *Geochemistry, Geophysics, Geosystems*, *14*(3), 489–518. doi: 10.1029/2012gc004334

Genske, F. S., Turner, S. P., Beier, C., & Schaefer, B. F. (2012). The petrology and geochemistry of lavas from the Western Azores Islands of Flores and Corvo. *Journal of Petrology*, *53*(8), 1673–1708. doi: 10.1093/petrology/egs029

Ghiorso, M. S., & Evans, B. W. (2008). Thermodynamics of rhombohedral oxide solid solutions and a revision of the FE-TI two-oxide geothermometer and oxygen-barometer. *American Journal of Science*, *308*(9), 957–1039. doi: 10.2475/09.2008.01

Gill, J. B. (1981). *Orogenic Andesites and Plate Tectonics*, New York: Springer-Verlag. 390 pp.

Grégoire, M., Moine, B. N., O'Reilly, S. Y., Cottin, J. Y., & Giret, A. (2000). Trace element residence and partitioning in mantle xenoliths metasomatized by highly alkaline, silicate-and carbonate-rich melts (Kerguelen Islands, Indian Ocean). *Journal of Petrology*, *41*(4), 477–509.

Grocke, S. B., Cottrell, E., de Silva, S., & Kelley, K. A. (2016). The role of crustal and eruptive processes versus source variations in controlling the oxidation state of iron in Central Andean magmas. *Earth and Planetary Science Letters*, *440*, 92–104. doi: 10.1016/j.epsl.2016.01.026

Grove, T. L., Till, C. B., & Krawczynski, M. J. (2012). The role of H2O in subduction zone magmatism. *Annual Review of Earth and Planetary Sciences*, *40*(1), 413–439. doi: 10.1146/annurev-earth-042711-105310

Grove, T. L., Baker, M. B., Price, R. C., Parman, S. W., Elkins-Tanton, L. T., Chatterjee, N., & Muntener, O. (2005). Magnesian andesite and dacite lavas from Mt. Shasta, northern California: products of fractional crystallization of H2O-rich mantle melts. *Contributions to Mineralogy and Petrology*, *148* (5), 542–565. doi: 10.1007/s00410-004-0619-6

Gunnarsson, B., Marsh, B. D., & Taylor, H. P. (1998). Generation of Icelandic rhyolites:silicic lavas from Torfajökull central volcano, edited. *Journal of Volcanology and Geothermal Research*, *83*(1–2), 1–45.

Haggerty, S. (1976). Opaque mineral oxides in terrestrial igneous rocks. *Oxide Minerals: Short Course Notes*, *3*, 101–300.

Hartley, M. E., Shorttle, O., Maclennan, J., Moussallam, Y., & Edmonds, M. (2017). Olivine-hosted melt inclusions as an archive of redox heterogeneity in magmatic systems. *Earth and Planetary Science Letters*, *479*, 192–205. doi: https://doi.org/10.1016/j.epsl.2017.09.029.

Hasse, K. M., Stoffers, P., & Dieter Garbe-Schönberg, C. (1997). The petrogenetic evolution of lavas from Easter Island and neighbouring seamounts, near-ridge hotspot volcanoes in the SE Pacific, edited. *Journal of Petrology*, *38*(6), 785–813.

Hauri, E. H., & Hart, S. R. (1994). Constraints on melt migration from mantle plumes: a trace element study of peridotite

xenoliths from Savai'i, Western Samoa. *Journal of Geophysical Research: Solid Earth*, *99*(B12), 24301–24321.

Helz, R., Cottrell, E., Brounce, M. N., & Kelley, K. A. (2017). Olivine-melt relationships and syneruptive redox variations in the 1959 eruption of K⍰lauea Volcano as revealed by XANES. *Journal of Volcanology and Geothermic Research*, *333*, 1–14.

Herd, C. D. K. (2008). Basalts as probes of planetary interior redox state. *Reviews in Mineralogy and Geochemistry*, *68*, 527–553.

Hirschmann, M., Withers, A., Ardia, P., & Foley, N. (2012). Solubility of molecular hydrogen in silicate melts and consequences for volatile evolution of terrestrial planets. *Earth and Planetary Science Letters*, *345*, 38–48.

Howe, T. M., Lindsay, J. M., Shane, P., Schmitt, A. K., & Stockli, D. F. (2014). Re-evaluation of the Roseau Tuff eruptive sequence and other Ignimbrites in Dominica, Lesser Antilles. *Journal of Quaternary Science*, *29*(6), 531–546. doi: 10.1002/jqs.2723

Izbekov, P. E., Eichelberger, J. C., Patino, L. C., Vogel, T. A., & Ivanov, B. V. (2002). Calcic cores of plagioclase phenocrysts in andesite from Karymsky volcano: Evidence for rapid introduction by basaltic replenishment. *Geology*, *30*(9), 799–802. doi: 10.1130/0091-7613(2002)030<0799:ccoppi>2.0.co;2

Janiszewski, H. A., Abers, G. A., Shillington, D. J., & Calkins, J. A. (2013). Crustal structure along the Aleutian island arc: New insights from receiver functions constrained by active-source data. *Geochemistry, Geophysics, Geosystems*, *14*(8), 2977–2992. doi: 10.1002/ggge.20211

Jayasuriya, K. D., O'Neill, H. S., Berry, A. J., & Campbell, S. J. (2004). A Mossbauer study of the oxidation state of Fe in silicate melts. *American Mineralogist*, *89*(11–12), 1597–1609.

Kelemen, P. B., Yogodzindki, G. M., & Scholl, D. W. (2003). Along-strike variation in the Aleutian Island Arc: Genesis of high Mg# Andesite and Implications for continental crust. *Geophysical Monograph 138*, 223–277. doi: 10.1029/138GM11

Kelemen, P. B., Hanghoj, K., & Greene, A. R. (2007). One view of the geochemistry of subduction-related magmatic arcs, with an emphasis on primitive andesite and lower crust. In Turekian, K., & Holland, H. (eds.) *Treatise on Geochemistry*, Elsevier Ltd. 1–70.

Kelley, K. A., & Cottrell, E. (2009). Water and the oxidation state of subduction zone magmas. *Science*, *325*(5940), 605–607. doi: 10.1126/science.1174156

Kelley, K. A., & Cottrell, E. (2012). The influence of magmatic differentiation on the oxidation state of Fe in a basaltic arc magma. *Earth and Planetary Science Letters*, *329*, 109–121. doi: 10.1016/j.epsl.2012.02.010

Kennedy, G. C. (1955). Some aspects of the role of water in rock melts. *Geological Society of America Special Paper*, *62*, 489–504.

Klimm, K., Kohn, S. C., O'Dell, L. A., Botcharnikov, R. E., & Smith, M. E. (2012). The dissolution mechanism of sulphur in hydrous silicate melts. I: Assessment of analytical techniques in determining the sulphur speciation in iron-free to iron-poor glasses. *Chemical Geology*, *322–323*, 237–249. doi: 10.1016/j.chemgeo.2012.04.027

Kress, V. C., & Carmichael, I. S. E. (1991). The compressibility of silicate liquids containing Fe2O3 and the effect of composition, temperature, oxygen fugacity and pressure on their redox states. *Contributions to Mineralogy and Petrology*, *108*, 82–92.

Krzywinski, M., & Altman, N. (2013). Significance, P values and t-tests. *Nature Methods*, *10*(11), 1041–1042. doi: 10.1038/nmeth.2698

Kushiro, I. (1972). Effect of water on composition of magmas formed at high pressures. *Journal of Petrology*, *13*(2), 311–334.

Kyser, T. K., O'Neil, J. R., & Carmichael, I. S. E. (1981). Oxygen isotope thermometry of basic lavas and mantle nodules. *Contributions to Mineralogy and Petrology*, *77*(1), 11–23.

Larsen, J. F. (2006). Rhyodacite magma storage conditions prior to the 3430 yBP caldera-forming eruption of Aniakchak volcano, Alaska. *Contributions to Mineralogy and Petrology*, *152*(4), 523–540. doi: 10.1007/s00410-006-0121-4

Laubier, M., Grove, T. L., & Langmuir, C. H. (2014). Trace element mineral/melt partitioning for basaltic and basaltic andesitic melts: An experimental and laser ICP-MS study with application to the oxidation state of mantle source regions. *Earth and Planetary Science Letters*, *392*, 265–278. doi: 10.1016/j.epsl.2014.01.053

Le Voyer, M., Cottrell, E., Kelley, K. A., Brounce, M., & Hauri, E. H. (2015). The effect of primary versus secondary processes on the volatile content of MORB glasses: An example from the equatorial Mid-Atlantic Ridge (5° N–3° S). *Journal of Geophysical Research: Solid Earth*, *120*(1), 125–144.

Le Voyer, M., Hauri, E. H., Cottrell, E., Kelley, K. A., Salters, V. J. M., Langmuir, C. H., et al. (2018). Carbon fluxes and primary magma CO2 contents along the global mid-ocean ridge system. *Geochemistry, Geophysics, Geosystems*, *20*(3), 1387–1424. doi: 10.1029/2018GC007630

Lecuyer, C., & Ricard, Y. (1999). Long-term fluxes and budget of ferric iron: implication for the redox states of the Earth's mantle and atmosphere. *Earth and Planetary Science Letters*, *165*(2), 197–211.

Lee, C.-T., Brandon, A. D., & Norman, M. (2003). Vanadium in peridotites as a proxy for paleo-fO(2) during partial melting: Prospects, limitations, and implications. *Geochimica Et Cosmochimica Acta*, *67*(16), 3045–3064.

Lee, C.-T., Leeman, W. P., Canil, D., & Li, Z.-X. A. (2005). Similar V/Sc Systematics in MORB and Arc Basalts: Implications for the Oxygen Fugacities of their Mantle Source Regions. *Journal of Petrology*, *46*(11), 2313–2336. doi: 10.1093/petrology/egi056

Lee, C.-T. A., Lee, T. C., & Wu, C.-T. (2013). Modeling the compositional evolution of recharging, evacuating, and fractionating (REFC) magma chambers: Implications for differentiation of arc magmas. *Geochimica et Cosmochimica Acta*, *143*, 8–22. doi: 10.1016/j.gca.2013.08.009.

Lee, C.-T. A., Luffi, P., Le Roux, V., Dasgupta, R., Albarede, F., & Leeman, W. P. (2010). The redox state of arc mantle using Zn/Fe systematics. *Nature*, *468*(7324), 681–685.

Lee, C. T. A., Luffi, P., Chin, E. J., Bouchet, R., Dasgupta, R., Morton, D. M., et al. (2012). Copper systematics in arc

magmas and implications for crust-mantle differentiation. *Science*, *336*(6077), 64–68. doi: 10.1126/science.1217313

Levin, V., Park, J., Brandon, M., Lees, J., Peyton, V., Gordeev, E., & Ozerov, A. (2002). Crust and upper mantle of Kamchatka from teleseismic receiver functions. *Tectonophysics*, *358*(1–4), 233–265. doi: 10.1016/s0040-1951(02)00426-2

Li, J., Kornprobst, J., Vielzeuf, D., & Fabriès, J. (1995). An improved experimental calibration of the olivine-spinel geothermometer. *Chinese Journal of Geochemistry*, *14*(1), 68–77.

Luhr, J. F. (2000). The geology and petrology of Volcán San Juan (Nayarit, México) and the compositionally zoned Tepic Pumice. *Journal of Volcanology and Geothermal Research*, *95*, 109–156.

Luhr, J. F., & Carmichael, I. S. E. (1980). The Colima Volcanic complex, Mexico: I. Post-caldera andesite from Volcán Colima. *Contributions to Mineralogy and Petrology*, *71*, 343–372.

Mallmann, G., & O'Neill, H. S. C. (2007). The effect of oxygen fugacity on the partitioning of Re between crystals and silicate melt during mantle melting. *Geochimica et Cosmochimica Acta*, *71*(11), 2837–2857. doi: 10.1016/j.gca.2007.03.028

Mallmann, G., & O'Neill, H. S. C. (2009). The Crystal/Melt Partitioning of V during Mantle Melting as a Function of Oxygen Fugacity Compared with some other Elements (Al, P, Ca, Sc, Ti, Cr, Fe, Ga, Y, Zr and Nb). *Journal of Petrology*, *50*(9), 1765–1794. doi: 10.1093/petrology/egp053

Mallmann, G., & O'Neill, H. S. (2013). Calibration of an empirical thermometer and oxybarometer based on the partitioning of Sc, Y and V between olivine and silicate melt. *Journal of Petrology*, *54*(5), 933–949. doi: 10.1093/petrology/egt001

Mallmann, G., Burnham, A., & Fonseca, R. O. (2021). Mineral-melt partitioning of redox-sensitive elements. In: Neuville, D. R., Moretti, R. (eds.) *AGU Geophysical Monograph Redox variables and mechanisms in magmatism and volcanism*. Wiley.

Manalo, P. C., Dirnalanta, C.B., Faustino-Eslava, D. V., Ramos, N. T., Queano, K. L., & Yumul, G. P. (2015). Crustal thickness variation from a continental to an island arc terrane: Clues from the gravity signatures of the Central Philippines. *Journal of Asian Earth Sciences*, *104*, 205–214. doi: 10.1016/j.jseaes.2014.08.031

Mandeville, C. W., Carey, S., & Sigurdsson, H. (1996). Magma mixing, fractional crystallization and volatile degassing during the 1883 eruption of Krakatau volcano, Indonesia. *Journal of Volcanology and Geothermal Research*, *74*(3–4), 243–274.

Mazzullo, L. J., & Bence, A. (1976). Abyssal tholeiites from DSDP Leg 34: the Nazca plate. *Journal of Geophysical Research*, *81*(23), 4327–4351.

McGlashan, N., Brown, L., & Kay, S. M. (2008). Crustal thickness in the central Andes from teleseismically recorded depth phase precursors. *Geophysical Journal International*, *175*(3), 1013–1022. doi: 10.1111/j.1365-246X.2008.03897.x

McKenzie, D., & Onions, R. K. (1983). Mantle reservoirs and ocean island basalts. *Nature*, *301*(5897), 229–231.

Montelli, R., Nolet, G., Dahlen, F. A., & Masters, G. (2006). A catalogue of deep mantle plumes: New results from finite-frequency tomography. *Geochemistry, Geophysics, Geosystems*, *7*(11). doi: 10.1029/2006gc001248

Moussallam, Y., Edmonds, M., Scaillet, B., Peters, N., Gennaro, E., Sides, I., & Oppenheimer, C. (2016). The impact of degassing on the oxidation state of basaltic magmas: A case study of K⊠lauea volcano. *Earth and Planetary Science Letters*, *450*, 317–325.

Moussallam, Y., Oppenheimer, C., Scaillet, B., Gaillard, F., Kyle, P., Peters, N., et al. (2014). Tracking the changing oxidation state of Erebus magmas, from mantle to surface, driven by magma ascent and degassing. *Earth and Planetary Science Letters*, *393*, 200–209.

Moussallam, Y., Longpré, M.-A., McCammon, C., Gomez-Ulla, A., Rose-Koga, E. F., Scaillet, B., et al. (2019). Mantle plumes are oxidised. *Earth and Planetary Science Letters*, *527*. doi: 10.1016/j.epsl.2019.115798

Muir, D. D., Blundy, J. D., Rust, A. C., & Hickey, J. (2014). Experimental constraints on dacite pre-eruptive magma storage conditions beneath Uturuncu Volcano. *Journal of Petrology*, *55*(4), 749–767. doi: 10.1093/petrology/egu005

Mungall, J. E. (2002). Roasting the mantle: Slab melting and the genesis of major Au and Au-rich Cu deposits. *Geology*, *30*(10), 915–918.

Myers, C. E., & Eugster, H. P. (1983). The system Fe-Si-O: Oxygen buffer calibrations to 1500K. *Contributions to Mineralogy and Petrology*, *82*, 75–90.

Mysen, B. O. (2006). Redox equilibria of iron and silicate melt structure: Implications for olivine/melt element partitioning. *Geochimica et Cosmochimica Acta*, *70*(12), 3121–3138. doi: 10.1016/j.gca.2006.03.014

Mysen, B. O., Kumamoto, K., Cody, G. D., & Fogel, M. L. (2011). Solubility and solution mechanisms of C–O–H volatiles in silicate melt with variable redox conditions and melt composition at upper mantle temperatures and pressures. *Geochimica et Cosmochimica Acta*, *75*, 6183–6199. doi: 10.1016/j.gca.2011.07.035

Nebel, O., Sossi, P. A., Bénard, A., Wille, M., Vroon, P. Z., & Arculus, R. J. (2015). Redox-variability and controls in subduction zones from an iron-isotope perspective. *Earth and Planetary Science Letters*, *432*, 142–151. doi: 10.1016/j.epsl.2015.09.036

Nell, J., & Wood, B. J. (1991). High-temperature electrical measurements and thermodynamic properties of Fe_3O_4-$FeCr_2O_4$-$MgCr_2O_4$-$FeAl_2O_4$ spinels. *American Mineralogist*, *76*(3–4), 405–426.

Neumann, E.-R. (1991). Ultramafic and mafic xenoliths from Hierro, Canary Islands: evidence for melt infiltration in the upper mantle. *Contributions to Mineralogy and Petrology*, *106*(2), 236–252.

Neumann, E. R., Wulff-Pedersen, E., Pearson, N. J., & Spencer, E. A. (2002). Mantle xenoliths from Tenerife (Canary Islands): evidence for reactions between mantle peridotites and silicic carbonatite melts inducing Ca metasomatism. *Journal of Petrology*, *43*(5), 825–857.

Neumann, E. R., Wulff-Pedersen, E., Johnsen, K., Andersen, T., & Krogh, E. (1995). Petrogenesis of spinel harzburgite and dunite suite xenoliths from Lanzarote, eastern Canary

Islands: implications for the upper mantle. *Lithos*, *35*(1–2), 83–107.

Newcombe, M., Brett, A., Beckett, J., Baker, M., Newman, S., Guan, Y., et al. (2017). Solubility of water in lunar basalt at low PH2O. *Geochimica et Cosmochimica Acta*, *200*, 330–352.

Nicklas, R. W., Puchtel, I. S., Ash, R. D., Piccoli, P. M., Hanski, E., Nisbet, E. G., et al. (2019). Secular mantle oxidation across the Archean-Proterozoic boundary: Evidence from V partitioning in komatiites and picrites. *Geochimica et Cosmochimica Acta*, *250*, 49–75. doi: 10.1016/j.gca.2019.01.037

Nicolich, R., Laigle, M., Hirn, A., Cernobori, L., & Gallart, J. (2000). Crustal structure of the Ionian margin of Sicily: Etna Volcano in the Fram of regional evolution. *Tectonophysics*, *329*, 121–139.

O'Neill, H. S., & Powncebу, M. I. (1993). Thermodynamic data from redox reactions at high temperatures. 1. An experimental and theoretical assessment of the electrochemical method using stabilized zirconia electrolytes, with revised values for the Fe- FeO, Co-CoO, Ni-NiO and Cu-Cu_2O oxygen buffers, and new data for the W-WO_2 buffer. *Contributions to Mineralogy and Petrology*, *114*(3), 296–314.

O'Neill, H. S. C., & Wall, V. (1987). The olivine–orthopyroxene–spinel oxygen geobarometer, the nickel precipitation curve, and the oxygen fugacity of the Earth's upper mantle. *Journal of Petrology*, *28*(6), 1169–1191.

O'Neill, H. S. C., Berry, A. J., & Mallmann, G. (2018). The oxidation state of iron in Mid-Ocean Ridge Basaltic (MORB) glasses: Implications for their petrogenesis and oxygen fugacities. *Earth and Planetary Science Letters*, *504*, 152–162. doi: 10.1016/j.epsl.2018.10.002

O'Neill, H. S. C. (1987). Quartz-fayalite-rion and quartz-fayalite-magnetite equilibria and the free energy of formation of fayalite (Fe_2SiO_4) and magnetite (Fe_3O_4). *American Mineralogist*, *72*, 67–75.

Osborn, E. F. (1959). Role of oxygen pressure in the crystallization and differentiation of basaltic magma. *American Journal of Science*, *257*(9), 609–647.

Parkinson, I. J., & Pearce, J. A. (1998). Peridotites from the Izu–Bonin–Mariana forearc (ODP Leg 125): evidence for mantle melting and melt–mantle interaction in a supra-subduction zone setting. *Journal of Petrology*, *39*(9), 1577–1618.

Parkinson, I. J., & Arculus, R. J. (1999). The redox state of subduction zones: insights from arc-peridotites. *Chemical Geology*, *160*(4), 409–423.

Parkinson, I. J., Arculus, R. J., & Eggins, S. M. (2003). Peridotite xenoliths from Grenada, Lesser Antilles Island Arc. *Contributions to Mineralogy and Petrology*, *146*(2), 241–262. doi: 10.1007/s00410-003-0500-z

Partzsch, G. M., Lattard, D., & McCammon, C. (2004). Mössbauer spectroscopic determination of Fe3+/Fe2+ in synthetic basaltic glass: a test of empirical fO_2 equations under superliquidus and subliquidus conditions. *Contributions to Mineralogy and Petrology*, *147*(5), 565–580. doi: 10.1007/s00410-004-0571-5

Pearce, J. A., Barker, P. F., Edwards, S. J., Parkinson, I. J., & Leat, P. T. (2000). Geochemistry and tectonic significance of peridotites from the South Sandwich arc-basin system, South Atlantic. *Contributions to Mineralogy and Petrology*, *139*, 36–53.

Plank, T., & Langmuir, C. H. (1988). An evaluation of the global variations in the major element chemistry of arc basalts. *Earth and Planetary Science Letters*, *90*(4), 349–370.

Plank, T., Kelley, K. A., Zimmer, M. M., Hauri, E. H., & Wallace, P. J. (2013). Why do mafic arc magmas contain 4 wt% water on average? *Earth and Planetary Science Letters*, *364*, 168–179. doi: 10.1016/j.epsl.2012.11.044

Portnyagin, M., Hoernle, K., Storm, S., Mironov, N., van den Bogaard, C., & Botcharnikov, R. (2012). H2O-rich melt inclusions in fayalitic olivine from Hekla volcano: Implications for phase relationships in silicic systems and driving forces of explosive volcanism on Iceland. *Earth and Planetary Science Letters*, *357–358*(0), 337–346. doi: 10.1016/j.epsl.2012.09.047

Righter, K., Danielson, L. R., Pando, K., Morris, R. V., Graff, T. G., Agresti, D. G., et al. (2013). Redox systematics of martian magmas with implications for magnetite stability. *American Mineralogist*, *98*(4), 616–628.

Rowe, M. C., Kent, A. J. R., & Nielsen, R. L. (2007). Determination of sulfur speciation and oxidation state of olivine hosted melt inclusions. *Chemical Geology*, *236*(3–4), 303–322.

Rutherford, M. J., & Devine, J. D. (1996). Preeruption pressure–temperature conditions and volatiles in the 1991 dacitic magma of Mount Pinatubo. In: Punongbayan, R., & Newhall, C. G. (eds.) *Fire and Mud: Eruptions and Lahars of Mount Pinatubo, Phillipines*. University of Washington Press. 751–766.

Ryabchikov, J. D., Ntaflos, T., Kurat, G., & Kogarko, L. N. (1995). Glass-bearing xenoliths from Cape Verde: evidence for a hot rising mantle jet. *Mineralogy and Petrology*, *55*(4), 217–237.

Sack, R. O., & Ghiorso, M. S. (1991a). Chromian spinels as petrogenetic indicators: Thermo dynamics and petrological applications. *American Mineralogist*, *76*, 827–847.

Sack, R. O., & Ghiorso, M. S. (1991b), An internally consistent model for the thermodynamic properties of Fe−Mg-titanomagnetite-aluminate spinels. *Contributions to Mineralogy and Petrology*, *106*(4), 474–505.

Saiga, A., Matsumoto, S., Uehira, K., Matsushima, T., & Shimizu, H. (2010). Velocity structure in the crust beneath the Kyushu area. *Earth Planets and Space*, *62*(5), 449–462. doi: 10.5047/eps.2010.02.003

Sen, G. (1987). Xenoliths associated with the Hawaiian Hot Spot. *Mantle Xenoliths*, 359–375.

Sen, G. (1988). Petrogenesis of spinel lherzolite and pyroxenite suite xenoliths from the Koolau shield, Oahu, Hawaii: implications for petrology of the post-eruptive lithosphere beneath Oahu. *Contributions to Mineralogy and Petrology*, *100*(1), 61–91.

Sen, G., & Presnall, D. C. (1986). Petrogenesis of dunite xenoliths from Koolau volcano, Oahu, Hawaii: implications for Hawaiian volcanism. *Journal of Petrology*, *27*(1), 197–217.

Sen, G., & Leeman, W. P. (1991). Iron-rich lherzolitic xenoliths from Oahu: origin and implications for Hawaiian magma sources. *Earth and Planetary Science Letters*, *102*(1), 45–57.

Sevilla, W. I., Ammon, C. J., Voight, B., & De Angelis, S. (2010). Crustal structure beneath the Montserrat region of

the Lesser Antilles island arc. *Geochemistry Geophysics Geosystems*, *11*, 13. doi: 10.1029/2010gc003048

Shervais, J. W. (1982). Ti-V plots and the petrogenesis of modern and ophiolitic lavas. *Earth and Planetary Science Letters*, *59*, 101–118.

Shorttle, O., Moussallam, Y., Hartley, M. E., Maclennan, J., Edmonds, M., & Murton, B. J. (2015). Fe-XANES analyses of Reykjanes Ridge basalts: Implications for oceanic crust's role in the solid Earth oxygen cycle. *Earth and Planetary Science Letters*, *427*, 272–285. doi: 10.1016/j.epsl.2015.07.017

Sleep, N. H. (1992). Hotspots and mantle plumes. *Annual Review of Earth Planetary Science*, *20*, 19–43.

Sorbadere, F., Laurenz, V., Frost, D. J., Wenz, M., Rosenthal, A., McCammon, C., & Rivard, C. (2018). The behaviour of ferric iron during partial melting of peridotite. *Geochimica et Cosmochimica Acta*, *239*, 235–254. doi: 10.1016/j.gca.2018.07.019

Spieker, K., Rondenay, S., Ramalho, R., Thomas, C., & Helffrich, G. (2018). Constraints on the structure of the crust and lithosphere beneath the Azores Islands from tele seismic receiver functions. *Geophysical Journal International*, *213*, 824–835.

Stagno, V., Ojwang, D. O., McCammon, C. A., & Frost, D. J. (2013). The oxidation state of the mantle and the extraction of carbon from Earth's interior. *Nature*, *493*(7430), 84–88. doi: 10.1038/nature11679

Stelten, M. E., & Cooper, K. M. (2012). Constraints on the nature of the subvolcanic reservoir at South Sister volcano, Oregon from U-series dating combined with sub-crystal trace-element analysis of plagioclase and zircon. *Earth and Planetary Science Letters*, *313*, 1–11. doi: 10.1016/j.epsl.2011.10.035

Stolper, D. A., & Bucholz, C. E. (2019). Neoproterozoic to early Phanerozoic rise in island arc redox state due to deep ocean oxygenation and increased marine sulfate levels. *Proceedings of the National Academy of Sciences of the United States of America*, *116*(18), 8746–8755. doi: 10.1073/pnas.1821847116

Stolper, E., & Newman, S. (1994). The role of water in the petrogenesis of Mariana Trough magmas. *Earth and Planetary Science Letters*, *121*(3–4), 293–325.

Stracke, A., Hofmann, A. W., & Hart, S. R. (2005). FOZO, HIMU, and the rest of the mantle zoo. *Geochemistry, Geophysics, Geosystems*, *6*, Q05007.

Syuhada, S., Hananto, N. D., Abdullah, C. I., Puspito, N. T., Anggono, T., & Yudistira, T. (2016). Crustal structure along Sunda-Banda arc transition zone from teleseismic receiver functions. *Acta Geophysica*, *64*, 2020–2049.

Takahashi, N., Kodaira, S., Klemperer, S. L., Tatsumi, Y., Kaneda, Y., & Suyehiro, K. (2007). Crustal structure and evolution of the Mariana intra-oceanic island arc. *Geology*, *35*(3), 203–206.

Tang, M., Erdman, M., Eldridge, G., & Lee, C. A. (2018). The redox "filter" beneath magmatic orogens and the formation of continental crust. *Science Advances*, *4*.

Thornber, C. R., Roeder, P. L., & Foster, J. R. (1980). The effect of composition on the ferric-ferrous ratio in basaltic liquids at atmospheric pressure. *Geochimica et Cosmochimica Acta*, *44* (3), 525–532.

Tollan, P., & Hermann, J. (2019). Arc magmas oxidised by water dissociation and hydrogen incorporation in orthopyroxene. *Nature Geoscience*, *12*(8), 667–671. doi: 10.1038/s41561-019-0411-x

Toothill, J., Williams, C. A., Macdonald, R., Turner, S. P., Rogers, N. W., Hawkesworth, C. J., et al. (2007). A complex petrogenesis for an arc magmatic suite, St Kitts, Lesser Antilles. *Journal of Petrology*, *48*(1), 3–42. doi: 10.1093/petrology/egl052

Tracy, R. J. (1980). Petrology and genetic significance of an ultramafic xenolith suite from Tahiti. *Earth and Planetary Science Letters*, *48*(1), 80–96.

Tucker, J. M., Hauri, E. H., Marske, J. P., Garcia, M. O., Trusdell, M. A., & Pietruszka, A. J. (2019). A high carbon content of the Hawaiian mantle from olivine-hosted melt inclusions. *Geochimica et Cosmochimica Acta*, *254*, 156–172.

Turner, S. J., & Langmuir, C. H. (2015). The global chemical systematics of arc front stratovolcanoes: Evaluating the role of crustal processes. *Earth and Planetary Science Letters*, *422*, 182–193. doi: 10.1016/j.epsl.2015.03.056

Turner, S. J., & Langmuir, C. (2015). What processes control the chemical compositions of arc front stratovolcanoes? *Geochemistry, Geophysics, Geosystems*, *16*, 1865–1893. doi: 10.1002/2014GC005633

Turner, S. J., Langmuir, C., Katz, R. F., Dungan, M. A., & Escrig, S. (2016). Parental arc magma compositions dominantly controlled by mantle-wedge thermal structure. *Nature Geoscience*, *9*, 772–776. doi: 10.1038/ngeo2788

Veenstra, E., Christensen, D. H., Abers, G. A., & Ferris, A. (2006). Crustal thickness variation in south-central Alaska. *Geology*, *34*(9), 781–784. doi: 10.1130/g22615.1

Wallace, P. J., & Carmichael, I. S. E. (1994). S-Speciation in submarine basaltic glasses as determined by measurements of Sk-Alpha x-ray wavelength shifts. *American Mineralogist*, *79* (1–2), 161–167.

Wasilewski, B., Doucet, L. S., Moine, B., Beunon, H., Delpech, G., Mattielli, N., et al. (2017). Ultra-refractory mantle within oceanic plateau: Petrology of the spinel harzburgites from Lac Michèle, Kerguelen Archipelago. *Lithos*, *272*, 336–349.

Waters, L. E., & Lange, R. A. (2013). Crystal-poor, multiply saturated rhyolites (obsidians) from the Cascade and Mexican arcs: evidence of degassing-induced crystallization of phenocrysts. *Contributions to Mineralogy and Petrology*, *166*(3), 731–754. doi: 10.1007/s00410-013-0919-9

Waters, L. E., & Lange, R. A. (2015). An updated calibration of the plagioclase-liquid hygrometer-thermometer applicable to basalts through rhyolites. *American Mineralogist*, *100*(10), 2172–2184. doi: 10.2138/am-2015-5232

Waters, L. E., & Lange, R. A. (2016). No effect of H2O degassing on the oxidation state of magmatic liquids. *Earth and Planetary Science Letters*, *447*, 48–59. doi: 10.1016/j.epsl.2016.04.030

Waters, L. E., & Frey, H. M. (2018). Crystal-poor rhyolites and rhyodacites from Volcan Tepetiltic, Mexico: Evidence for melt formation, crystallization and eruption over short timescales. *Journal of Volcanology and Geothermal Research*, *361*, 36–50. doi: 10.1016/j.jvolgeores.2018.08.003

Watts, A. B., & ten Brink, U. S. (1989). Crustal structure, flexure, and subsidence history of the Hawaiian Islands. *Journal of Geophysical Research Solid Earth*, *94*, 10473–10500.

Wilke, M., Jugo, P. J., Klimm, K., Susini, J., Botcharnikov, R., Kohn, S. C., & Janousch, M. (2008). The origin of S4+ detected in silicate glasses by XANES. *American Mineralogist*, *93*(1), 235–240. doi: 10.2138/am.2008.2765

Williams, H., Peslier, A., McCammon, C., Halliday, A., Levasseur, S., Teutsch, N., & Burg, J. (2005). Systematic iron isotope variations in mantle rocks and minerals: The effects of partial melting and oxygen fugacity. *Earth and Planetary Science Letters*, *235*(1–2), 435–452. doi: 10.1016/j.epsl.2005.04.020

Williams, H. M., McCammon, C. A., Peslier, A. H., Halliday, A. N., Teutsch, N., Levasseur, S., & Burg, J.-P. (2004). Iron isotope fractionation and the oxygen fugacity of the mantle. *Science*, *304*(5677), 1656–1659.

Wolfe, E. W., Wise, W. S., & Dalrymple, G. B. (1997). The geology and petrology of Mauna Kea Volcano, Hawaii – A study of postshield volcanism. USGS Professional Paper. pp. 1–129.

Wood, B. J. (1990). An experimental test of the spinel peridotite oxygen barometer. *Journal of Geophysical Research-Solid Earth and Planets*, *95*(B10), 15845–15851.

Wood, B. J., & Virgo, D. (1989). Upper mantle oxidation state – ferric iron contents of lherzoline spinels by Fe-57 Mossbauer spectroscopy and resultant oxygen fugacities. *Geochimica et Cosmochimica Acta*, *53*(6), 1277–1291.

Wood, B. J., Bryndzia, L. T., & Johnson, K. E. (1990). Mantle oxidation-state and its relationship to tectonic environment and fluid speciation. *Science*, *248*(4953), 337–345.

Wulff-Pedersen, E., Neumann, E.-R., & Jensen, B. á. (1996). The upper mantle under La Palma, Canary Islands: formation of Si- K- Na-rich melt and its importance as a metasomatic agent. *Contributions to Mineralogy and Petrology*, *125*(2–3), 113–139.

Zhang, H. L., Cottrell, E., Solheid, P. A., Kelley, K. A., & Hirschmann, M. M. (2018). Determination of Fe3+/SFe of XANES basaltic glass standards by Mössbauer spectroscopy and its application to the oxidation state of iron in MORB. *Chemical Geology*, *479*(2018), 166–175.

Zimmer, M. M., Plank, T., Hauri, E. H., Yogodzinski, G. M., Stelling, P., Larsen, J., et al. (2010). The role of water in generating the calc-alkaline trend: New volatile data for Aleutian magmas and a new tholeiitic index. *Journal of Petrology*, *51*(12), 2411–2444. doi: 10.1093/petrology/egq062